

Review on the Design of the Isolation Techniques for UWB-MIMO Antennas

G. Irene* and A. Rajesh

Department of Communication Engineering, School of Electronics Engineering
VIT University, Vellore

*corresponding author, E-mail: irenesuriya@gmail.com

Abstract

Ultra wideband - Multiple Input Multiple Output antenna technologies provide higher data rates and the combination of the ultra-wideband (UWB) and the multiple input multiple output (MIMO) technologies provide a solution for the demand of still higher data rates i.e. in excess of 3 Gb/sec in the future. As the antenna technologies are improving, the size of the MIMO antenna is growing smaller and smaller. Placing the antenna elements in such close proximity increases the coupling between them. Various isolation techniques have to be introduced between the antenna elements to decrease the coupling and to improve the isolation. A study of the various isolation enhancement techniques has been made in this review. It analyses the various isolation enhancement methods such as by using orthogonal polarization, parasitic elements, decoupling structures, defected ground structures (DGS), neutralization line (NL) and finally by using metamaterials. Metamaterials is a technology to perk up the isolation between the antenna elements. Split ring resonator (SRR) behaves as a metamaterial and it is used as an isolation mechanism in this study. The antennas are simulated and the results are compared. The method using the parasitic elements is the best isolation mechanism. The method using parasitic elements gives the highest isolation of 35 dB and it is 5 dB better than the methods using orthogonal polarization and by using the decoupling structure. The performance of all the antennas satisfies the conditions for minimum isolation. The envelope correlation coefficient is nearly zero in all the antennas and it implies good diversity performance. The diversity gain is also calculated for the various antennas and it satisfies good diversity performance. The bandwidth of the antennas is in the UWB frequency range and they have a fractional bandwidth above the required value of 1.09. The capacity loss for all the antennas is very low and the antennas using defected ground structure and the decoupling structure gives a very low capacity loss.

I. INTRODUCTION

As the quantity of applications and the number of users utilizing wireless communications is expanding, thereby the amount of data rate used is dynamically expanding. As of now, WLANs offers rates up to 54 Mb/s and in the near future, an objective of 600 Mb/s is to be realized. The emerging WLANs such as home audio/video network applications, high-speed high definition television (HDTV) audio/video streams requires 1 Gb/s transmission rates. To accomplish, data rates of more than 50 Mb/sec, MIMO and OFDM technologies are embraced as recommended in IEEE 802.11n. To achieve the objective of 1 Gb/sec, advanced

techniques such as UWB combined with MIMO provides the solution [1-2]. For the future technologies such as IEEE 802.15.3c wireless personal area networks (WPANs) utilizing a data rate of over 2 Gb/sec and for data rates in excess of 3 Gb/sec, the combination of MIMO and UWB technologies provides the necessary solution.

High data rate communications are possible using UWB and it provides an excellent technology for short-range wireless communications. Using UWB there is a number of applications, especially in the wireless world. The main applications of UWB are sensor networks, WBAN, RFIDs, WPAN, radars, etc. In 2002, the frequency range from 3.1 to 10.6 GHz was regulated by FCC, for the utilization of UWB. UWB is needed for high data rate communications, especially for commercial applications. In the USA and in Asia, UWB system makes use of the wide frequency band ranging from 3.1 to 10.6 GHz and from 6.0 to 8.5 GHz in Europe. But FCC imposes a limit on the permitted power spectral density which limits the data transmission rates. The main advantages of (UWB) are simultaneous multiple user channels, tremendous data rate, extremely low level of radiation, and reduced probability of detection, thus it has become an important field of research.

Multiple-Input-Multiple-Output (MIMO) has risen to a standard of revolutionary importance in digital communications and it has created a breakthrough in the systems using wireless technology. The main disadvantages of wireless systems are signal fading, increasing interference, multipath, and limited spectrum. Without consuming extra radio frequency, MIMO technology provides higher data throughput along with an increase in range and reliability by exploiting multipath. The antenna diversity techniques such as polarization, spatial, and pattern diversity is exploited by MIMO to enhance the power of the transmitted signals, and thereby it enhances the signal to noise ratio (SNR). STC (Space Time Coding) and beamforming techniques are useful in this regard. Using STC the overall transmitted power remains the same while the power of an individual transmitted symbol is strengthened. The beamforming technique increases the power of the signal in a specific direction.

On the other hand, an efficient UWB antenna is obtained by introducing techniques that will reject the bands that will interfere with the UWB frequency. An excellent ultra-wideband MIMO antenna should be able to isolate the interfering bands and also should have high isolation characteristics between the antenna elements. An efficient antenna having these characteristics should be designed in the limited area provided.

II. PARAMETERS OF UWB-MIMO ANTENNA

When designing an ultra-wideband MIMO antenna, there is a number of challenges to be addressed. Some of the parameters that are used in performance evaluation of the MIMO antenna [1] are:

A. Total Active Reflection Coefficient

To achieve better characterization of the efficiency and bandwidth of the MIMO antenna, total active reflection coefficient (TARC) is used. TARC is given by the ratio of the square root of the total reflected power and the square root of the total incident power. TARC is obtained by manipulating all of the S-parameters for an N-port network and it displays a single curve having all the information of the S-parameters. TARC is calculated as [1],

$$\Gamma_a^t = \frac{\sqrt{\sum_{i=1}^N |b_i|^2}}{\sqrt{\sum_{i=1}^N |a_i|^2}} \quad [1]$$

where a_i is the incident signals and b_i is the reflected signals. These are obtained from the measured S-parameters. The reference line for the calculation of TARC is -10 dB.

B. Isolation

The coupling between the adjacent antenna elements within the MIMO antenna in terms of electromagnetic energy is measured by isolation. It is an important parameter that measures the coupling in the structure of the antenna and not the coupling through the radiation patterns. The value of isolation should be greater than 15 dB. Lower the coupling between the antenna elements, higher the isolation obtained [1].

$$\text{Isolation} = -10 \log_{10} |S_{21}|^2 \quad [2]$$

where S_{21} refer to the amount of power transferred from port 1 to port 2.

C. Envelope Correlation Coefficient

The correlation between the antenna elements is measured by the correlation coefficient. It measures how much the radiation patterns of the antenna elements affect one another when they are operated simultaneously. The square of the correlation coefficient gives the envelope correlation coefficient (ECC). It can also be evaluated from the S-parameters [1].

$$\rho_e = \frac{\left| \iint_{4\pi} [\bar{F}_1(\theta, \varphi) * \bar{F}_2(\theta, \varphi)] d\Omega \right|^2}{\iint_{4\pi} |\bar{F}_1(\theta, \varphi)|^2 d\Omega \iint_{4\pi} |\bar{F}_2(\theta, \varphi)|^2 d\Omega} \quad [3]$$

where Ω is the solid angle and when the i^{th} port is excited the 3D field radiation pattern of the antenna is given by $\bar{F}_i(\theta, \varphi)$. The envelope correlation coefficient can also be calculated from the S-parameters and the radiation efficiency of the antenna. The envelope correlation coefficient between i and j elements is given by [1],

$$\rho_e = \left| \frac{|S_{ii}^* S_{ij} + S_{ji}^* S_{jj}|}{\left[(1 - |S_{ii}|^2 - |S_{ji}|^2)(1 - |S_{jj}|^2 - |S_{ij}|^2) \right]^{1/2}} \right|^2 \quad [4]$$

For the antenna to show good diversity conditions, the value of 0.5 has been set as the upper limit. High isolation and near zero correlation coefficient are required for a MIMO antenna with good diversity performance.

D. Mean Effective Gain

The performance of the antenna in a predefined wireless environment is measured by the mean effective gain (MEG). In MEG [1], the effect of the environment is taken into consideration to calculate the gain performance of the antenna. It is helpful in measuring the effect of the environment on the radiation characteristics of an antenna and it is important to evaluate the true performance of the antenna in the environment.

$$\text{MEG} = \int_0^{2\pi} \int_0^\pi \left(\frac{XPD}{1+XPD} G_\theta(\theta, \varphi) P_\theta(\theta, \varphi) + \frac{1}{1+XPD} G_\varphi(\theta, \varphi) P_\varphi(\theta, \varphi) \right) \sin \theta d\theta d\varphi \quad [5]$$

which satisfies the conditions

$$\begin{aligned} \int_0^{2\pi} \int_0^\pi [G_\theta(\theta, \varphi) + G_\varphi(\theta, \varphi)] \sin \theta d\theta d\varphi &= 4\pi \quad \text{and} \\ \int_0^{2\pi} \int_0^\pi P_\theta(\theta, \varphi) \sin \theta d\theta d\varphi &= \\ \int_0^{2\pi} \int_0^{2\pi} P_\varphi(\theta, \varphi) \sin \theta d\theta d\varphi &= 1 \end{aligned}$$

XPD [1] is the cross-polarization ratio

$$\text{XPD} = \frac{P_v}{P_H} \quad [6]$$

$$\text{where XPD} = \frac{\int_0^{2\pi} \int_0^\pi P_\theta(\theta, \varphi) \sin \theta d\theta d\varphi}{\int_0^{2\pi} \int_0^\pi P_\varphi(\theta, \varphi) \sin \theta d\theta d\varphi}$$

E. Diversity Gain

The effect of diversity which is usually achieved when the transmitter through different channel paths receives multiple versions of the transmitted stream. It is evaluated as the difference between the time-averaged SNR of the combined signals in a MIMO antenna and that of a single antenna system in a single antenna where the SNR is above a standard reference level.

$$\text{Diversity gain} = \left[\frac{\gamma_c}{SNR_c} - \frac{\gamma_1}{SNR_1} \right]_{P(\gamma_c < \gamma_s / SNR)} \quad [7]$$

Diversity gain [1] can be obtained from the envelope correlation coefficient as

$$DG = 10\sqrt{(1-|\rho|^2)} \quad [8]$$

The lower the correlation coefficient, higher the diversity gain.

F. Branch Power Ratio

The relative power levels that come from different antenna branches affects the MIMO antenna performance. Ideally, the difference of the power levels coming from various branches should be very low. A branch power level ratio, k is used to identify these differences in the power level and, is defined as [1],

$$k = \frac{P_{min}}{P_{max}} \quad [9]$$

where P_{min} is represented as the power of the antenna with the lower power, and P_{max} represents the power of the antenna with the higher power.

The diversity gain will be affected by the power level ratio, as the actual diversity gain is the product of the overall obtained diversity gain and the branch power level ratio. The MEG values can also be used to represent the branch power level ratio (k). For a two-element antenna system [1],

$$k = \min\left(\frac{MEG_2}{MEG_1}, \frac{MEG_1}{MEG_2}\right) \quad [10]$$

where MEG_1 and MEG_2 are the mean effective gain of antenna 1 and antenna 2. k should be between 0 and -3 dB, for the MIMO antenna to obtain maximum diversity gain and avoid a significant loss in the diversity performance.

G. System Capacity

The ideal channel limit of a MIMO system is obtained with the help of Shannon's capacity theorem. But due to the presence of correlation and mutual coupling between the antenna elements, this limit is never achieved. The capacity of the channel (C) in a wireless environment is calculated as a function of the radiation characteristics of the antenna elements and the channel environment [1].

$$C = \log_2 \left[\det \left(I_N + \frac{\rho}{N} H H^T \right) \right] \quad [11]$$

Correlation between the antenna elements decreases the MIMO capacity, and it induces a loss of capacity which is given by the capacity loss. The capacity loss for high SNR is given by

$$C (\text{Loss}) = -\log_2 \det(\varphi^R) \quad [12]$$

where φ^R is a 2x2 correlation matrix.

$$\varphi^R = \begin{bmatrix} \rho_{11} & \rho_{12} \\ \rho_{21} & \rho_{22} \end{bmatrix} = \rho_{ij} \quad [13]$$

where ρ_{ij} is the correlation coefficient between the antennas i and j in an $N \times N$ MIMO antenna.

The maximum value of the capacity loss is 0.5. Antennas having capacity loss below 0.5, have very low capacity loss and maximum capacity in the channel.

III. FACTORS AFFECTING ISOLATION

H. Polarization

Orthogonal polarization is achieved when two linearly polarized waves are perpendicular to each other. They do not interact with each other as they are orthogonal to each other and therefore are well isolated. Isolation between multiple antennas can be improved by placing the antennas in such a manner that the polarization of the antenna is orthogonal.

B. Antenna size

The size of an antenna is set by the Chu-Harrington limit. For a certain frequency, the minimum size of the antenna can be calculated if we know the bandwidth and efficiency, from the Chu-Harrington limit. It is also seen that antennas with linear polarization increase the size of the antenna whereas the antennas with orthogonal polarization are independent.

I. Separation and power patterns

The coupling between the antenna elements when they are widely separated is given by the path loss equation where the coupling is given by

$$\text{Coupling} = L + G_1 + G_2 \text{ (dB)},$$

where G_1 is the gain of the antenna 1 facing antenna 2. G_2 is the gain of antenna 2 facing antenna 1.

$$L = 32.4 + 20\log_{10}f \text{ (MHz)} + 20\log_{10}D \text{ (KM)}. \quad [14]$$

where L is the path loss between the antennas

Placing the two antennas close by will cause coupling due to the antennas' reactive near field. The directions of the highest reactive field and the direction of the far-field antenna need not be the same. And it can be seen that the strength of the far field has a lower drop off rate than the reactive near field.

UWB antennas can be equated to a series resonant RLC circuit, as it is represented as a series of narrowband antennas inside a working frequency [2]. The equivalent impedance at the input terminal can be considered as

$$Z_e = \sum_{i=1}^n \frac{j\omega R_i L_i}{R_i(1-\omega^2 L_i C_i) + j\omega L_i} \quad [15]$$

IV. SURFACE WAVE PROPAGATION AND GROUND PLANE CURRENTS

When an antenna is excited, currents are set up in the ground plane. Antennas such as monopoles which are widely used in ultra-wideband technology are driven directly from the ground plane and they excite the surface current in the ground plane. But, surface waves or ground plane current increases the coupling between the antennas. And efficient technology should be introduced to reduce the

surface wave flow. The size of the reactive near field also increases when a large portion of the ground plane is used for radiation. When two antennas are placed adjacent to each other, coupling takes place because of the reactive near-field also.

V. ISOLATION ENHANCEMENT TECHNIQUES IN UWB MIMO ANTENNA SYSTEMS

Development of MIMO antennas can be a challenge due to the small space between the antenna elements. This limits the diversity as the antenna elements are placed close together. So, the patterns are to be decorrelated or the mutual coupling is to be reduced. The isolation between the ports of the MIMO antenna should be increased.

J. Polarization diversity

The isolation between the antenna elements can be improved by using polarization diversity. Isolation is increased by orthogonally placing the linearly polarized antenna elements. Orienting the antenna elements orthogonally decreases the ground coupling and the field coupling. The phase of the coupling currents and the radiated field's polarization is disturbed due to the positioning of the antenna elements. In [3], a quasi-self-complementary antenna MIMO antenna is proposed. Polarization diversity is exploited in this antenna by placing the antenna elements orthogonally. Because of the presence of the self-complementary structure, high isolation is obtained without the addition of any decoupling structure. The isolation obtained is greater than 20 dB and the ECC obtained is less than 0.5. In [4], a dual-polarized UWB-MIMO antenna which is compact in size is proposed consisting of a single ultra-wideband monopole to which feeding is given by two meandering microstrip lines. Slots and stubs were used to reduce the mutual coupling. Meandering the microstrip feed line miniaturized the antenna structure. The RF currents are forced by the slots to concentrate on the edge of the antenna elements instead of coupling from the excited port to the other and it reduces the mutual coupling by more than 50%. The meandered microstrip lines help in reducing the mutual coupling.

A quarter wave open circuit stub which resonates at 5.5 GHz is shorted at one end of the ground. The leaked energy is shorted to the ground showing a band-stop filter behavior which is obtained by using a series inductance and shunt capacitance, thereby reducing the mutual coupling. The ECC obtained in the band of interest is <0.1 . The isolation obtained is greater than 20 dB. In [5], a MIMO antenna is proposed which consists of antenna elements consisting of stepped slots which resonate at various frequencies. Without the addition of any decoupling structure, improved isolation is obtained because of the radiation properties of the slot antenna which is an inherent property and also due to the asymmetric placement of the antenna elements. The isolation obtained is greater than 22 dB and the ECC obtained is 0.01. In [6], the antenna elements are orthogonally placed to enhance the isolation. Band-rejection of the WLAN wireless band is achieved by introducing a band-stop design which behaves as an LC band stop filter and changes the current path and thereby notches the desired frequency.

In [7], the antenna element consists of a monopole which is rectangular with an arced feeding section and the partial ground is utilized to achieve the required impedance

bandwidth. The second monopole was placed at a distance of 1 mm symmetrically, but it showed high mutual coupling, and when the second monopole was placed at 90° , to the first, the mutual coupling was reduced and high isolation was obtained. By exploiting polarization diversity, high isolation has been obtained. The antenna was designed on a low-loss Roger TMM4 laminate having dimensions with thickness 1.524 mm, having dielectric constant 4.5 and a loss tangent 0.002. The antenna in [7] was simulated in CST Microwave studio and the results were obtained. The top layer of the antenna and the bottom of the ground plane is as shown in Fig.1.

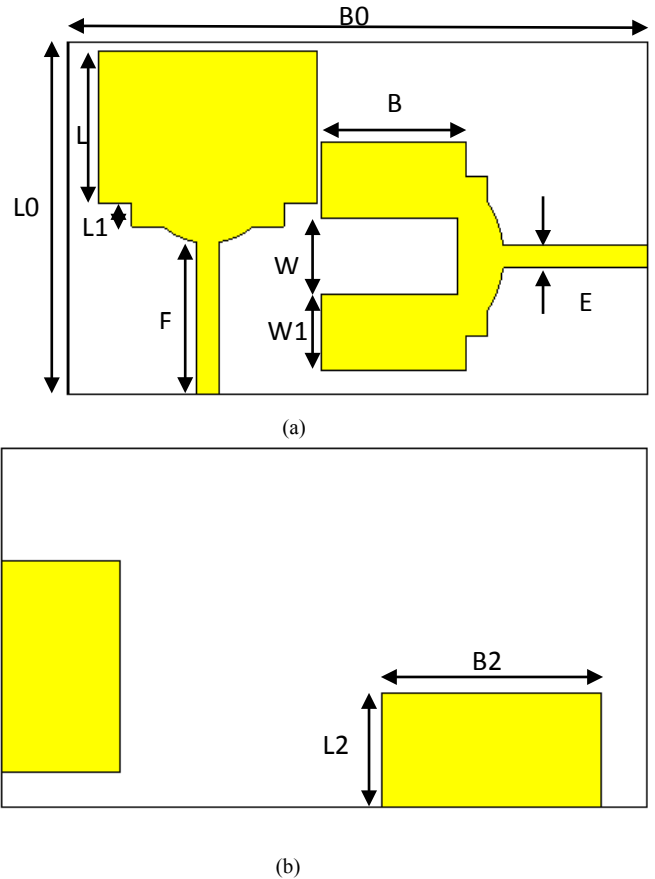


Fig.1 (a) top and (b) bottom layer of the orthogonally polarized antenna [7]

L0	B0	L	B	W	W1	L1	L2
23	39.8	10	10	5	5	1.5	6.25
B2	E	F					
13.5	1.5	9.85					

a. Equivalent circuit of the antenna

Useful insights regarding the performance of the antenna can be obtained from the equivalent circuit using the foster canonical form assuming no ohmic losses. For a UWB antenna, a large bandwidth is due to the overlapping of several adjacent resonances and can be represented as serially connected parallel RLC circuits [36]. This is obtained by transforming the resonant peaks of the simulated input impedance of reference UWB antenna into the equivalent parallel RLC resonant circuit connected in series. C_0 and L_0 account for the static antenna capacitance

and probe inductance [36]. The real part of the input impedance of S_{11} of the UWB MIMO antenna is shown in Fig. 2. From the real part of the input impedance of S_{11} from Fig. 2, it can be seen that the resonant peaks (parallel resonant modes) are at 4.2 GHz, 6.3 GHz and at 10.3 GHz in the UWB and each frequency is represented as a parallel RLC circuit connected in series. The equivalent circuit of the antenna is as represented in Fig. 3.

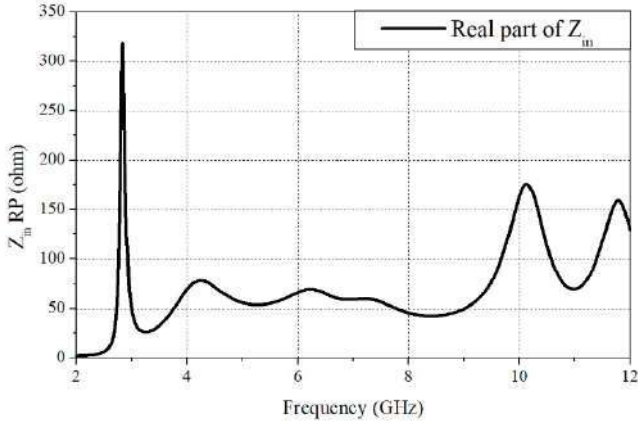


Fig. 2 Input impedance of the antenna

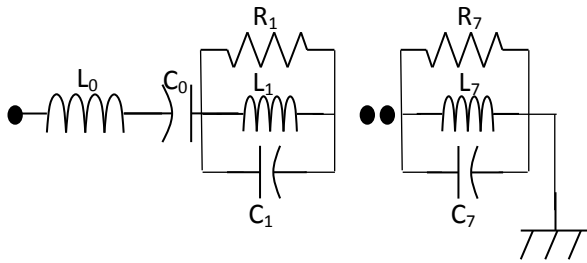


Fig. 3 Equivalent circuit of the antenna

Frequency (GHz)		4.2	6.3	10.13
R_n (Ω)		78.12	69.26	175.27
L_n (nH)	0.63	0.28	0.063	0.277
C_n (pF)	1.09	5.11	0.102	1.08

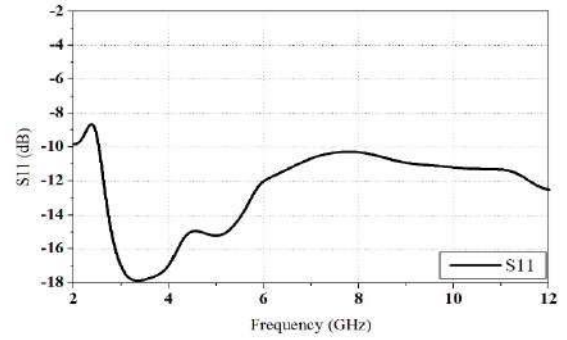
Table 1: Element values of the equivalent circuit

The parameters of the resistors, capacitors and inductors in the equivalent circuit are as shown in Table. 1 and are obtained using foster canonical forms. The parallel RLC network acts as a bandpass filter, thus creating a resonance A combination of the parallel RLC networks gives the desired UWB.

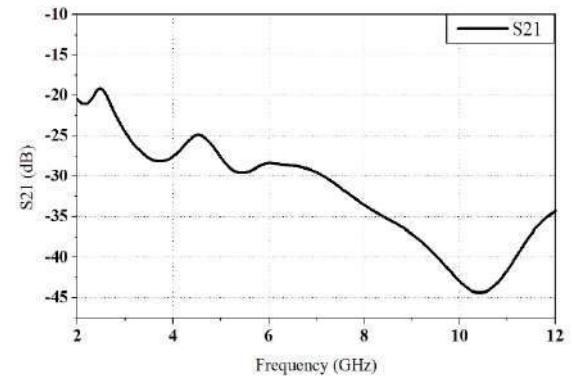
b. Simulated results

The orthogonally polarized MIMO antenna has a -10 dB bandwidth from 2.2 to 12 GHz as represented in Fig. 4(a). The isolation obtained between the antenna elements is -25 dB as represented in Fig. 4(b). The polarization purity of antenna 1 is high while the polarization of antenna 2 is low.

This is because of the U-shaped slot which decreases the power level of antenna element 2. The opposite sign of polarity in the power level difference shows that the antenna elements are orthogonally polarized. This mechanism helps to achieve good impedance bandwidth and isolation although the two elements are placed close to each other [7].

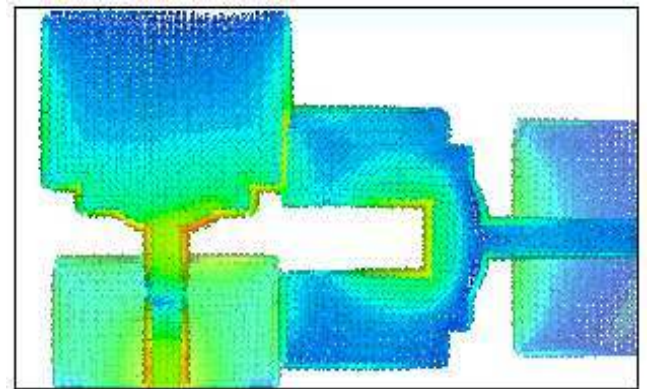


(a)

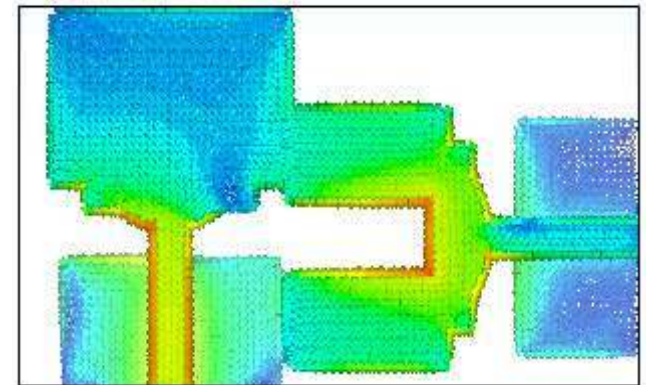


(b)

Fig.4 (a) S11 and (b) S21 of the antenna



(a)



(b)

Fig.5 Surface current distributions with port-1 excited at (a) 4 GHz and (b) 7.5 GHz

The current distributions at 4 GHz and at 7.5 GHz is as shown in the Fig.5. From the current distributions, when compared to the current distribution at 4 GHz, it can be seen that at 7.5 GHz, with port_1 excited, the isolation between the antenna elements is higher as the direction of current flow is in opposite directions. The current is also concentrated along the dimensions of the slot thereby reducing the coupling between the antenna elements.

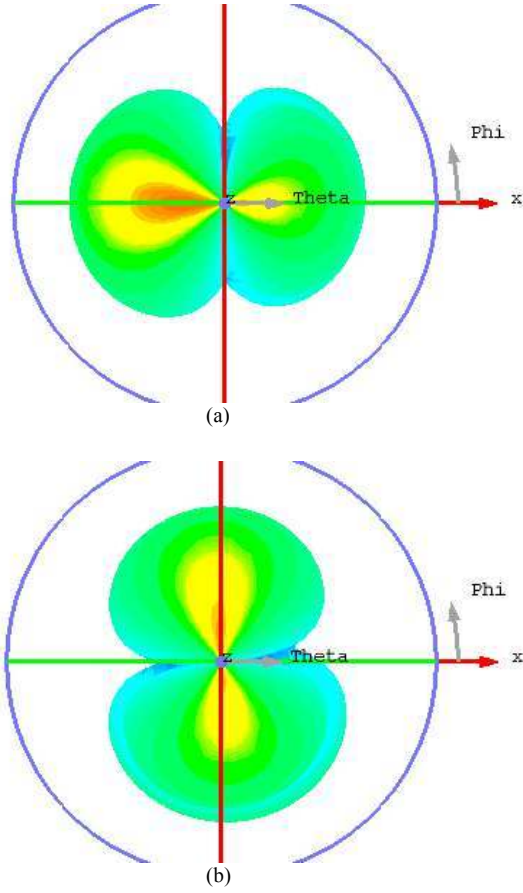


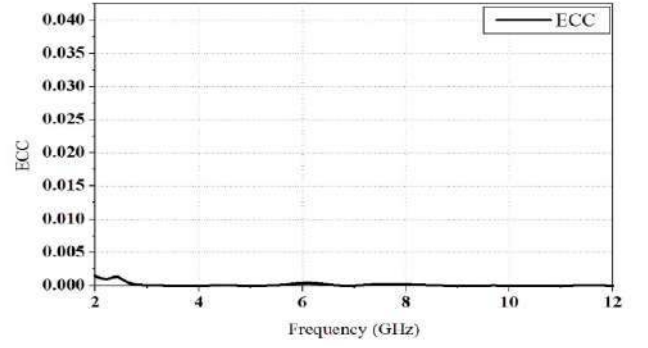
Fig.6 The radiation pattern at 5.5 GHz (a) with port_1 excited and (b) with port_2 excited

The radiation pattern of the MIMO antenna with port_1 excited is shown in Fig. 6(a) and with port_2 excited is shown in Fig. 6(b). It clearly shows that the patterns are orthogonally polarized, thereby improving the isolation in between the antenna elements. The ECC obtained is nearly equal to zero as shown in Fig. 57(a) and it has a small peak at 6 GHz and the diversity gain is nearly equal to 10 dB as shown in Fig. 7(b). It represents good diversity performance in the ultra-wideband frequency range [7]. The ECC is calculated by using the S-parameter method. The theoretical capacity of the MIMO antenna increases linearly with the number of antenna elements. But the capacity of the channel is reduced due to correlation.

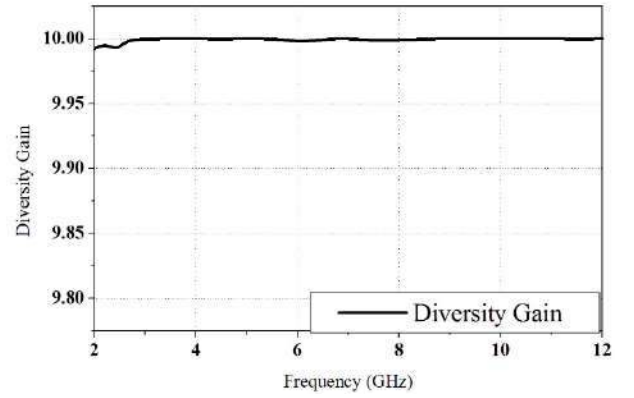
$$\rho_e = \left| \frac{|S_{ii}^* S_{ij} + S_{ji}^* S_{jj}|}{\left| (1 - |S_{ii}|^2 - |S_{ji}|^2)(1 - |S_{jj}|^2 - |S_{ij}|^2) \right|^{1/2}} \right|^2$$

This observation indicates that in rich multipath environments the corresponding signal paths are uncorrelated and are impossible to be in deep fade, simultaneously. This feature improves the performance of MIMO communication applications and systems [39]. From the radiation patterns obtained in Fig. 6, it can be seen that the antenna elements are uncorrelated with each other and hence the ECC is very low.

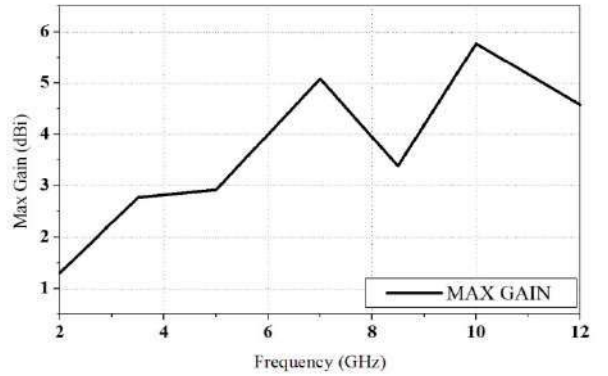
The gain of the antenna as shown in Fig. 7(c) is 3-4 dBi in the lower frequency band and 5-6 dBi in the upper band of the ultra-wide band frequency range.



(a)



(b)



(c)

Fig.7 (a) ECC of OP (b) diversity gain and (c) Maximum gain of the orthogonally polarized antenna structure

K. Parasitic elements

Parasitic elements are mainly used to reduce the coupling as it creates an opposing coupled field by terminating some of the couplings between the antenna elements and thereby reducing the RF current in the

neighboring antenna element. The bandwidth, the isolation range, and the surface current coupling can be controlled by designing a good parasitic element. In [8], a folded monopole MIMO antenna is proposed in which the coupling between the antenna elements is reduced by utilizing a meandered parasitic inverted-L element. The meandered parasitic element is actually a $\lambda/4$ wavelength line which is meandered to fit in into the antenna spacing. The coupling is reduced as the parasitic element functions as a reflector and thereby the radiation patterns are separated. An open stub is placed to achieve notched band frequency from 5.15-5.85 GHz.

In [9], the antenna comprises of two antenna elements that are orthogonally placed to achieve high isolation. The top and bottom layer of the antenna is as shown in Fig. 8. A parasitic T-shaped strip is used to further suppress the mutual coupling. The isolation obtained is greater than 15 dB and the ECC obtained is 0.02. Fig. 6 shows the antenna and the bottom of the ground plane. The dimensions of the substrate are $38.5 \times 38.5 \text{ mm}^2$ and the height of the substrate is 1.6 mm. It is designed on an FR4 substrate with loss tangent 0.02.

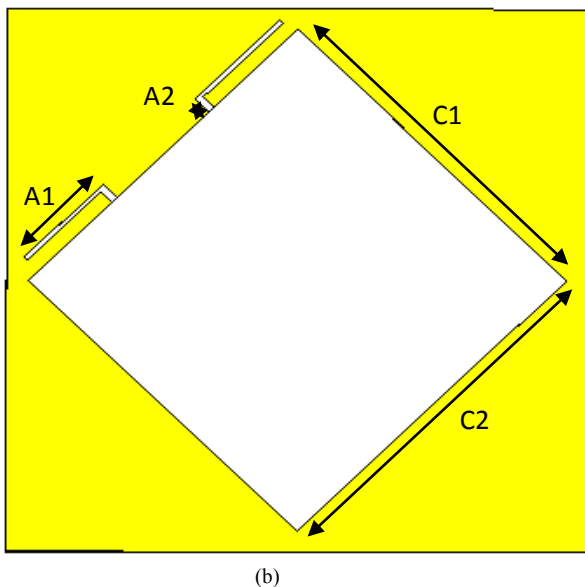
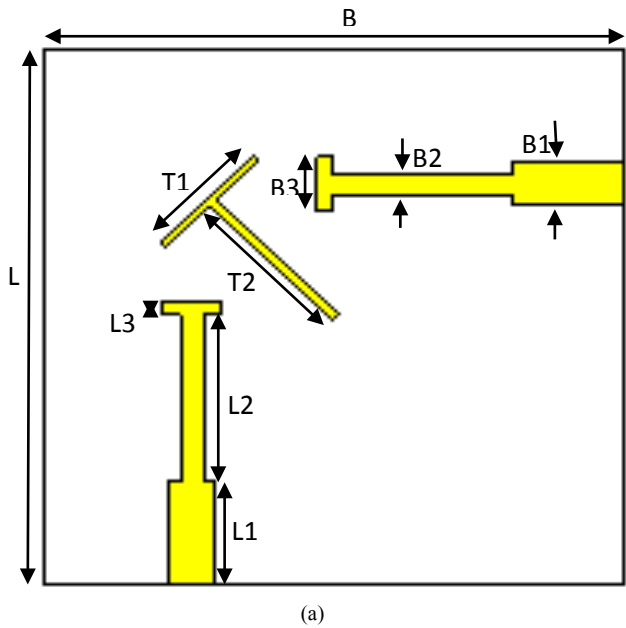


Fig. 8 (a) top and (b) bottom layer of the antenna [9]

L	B	L1	L2	L3	T1	T2	B1
38.5	38.5	7.4	12	1	8.8	11.5	3
B2	B3	A1	A2	C1	C2		
1.5	4	7.3	1	25.2	25.2		

a. Equivalent circuit of the antenna

The real part of the input impedance of S_{11} of the UWB MIMO antenna is shown in Fig. 9(a). From the real part of the input impedance of S_{11} from Fig. 9(a), it can be seen that the resonant peaks (parallel resonant modes) are at 3.26 GHz, 6.74 GHz, 7.32 GHz and at 9.59 GHz in the UWB and each frequency is represented as a parallel RLC circuit connected in series.

The band notched functions are realized according to conceptual circuit model by connecting the antenna input impedance with either a parallel or a series R-L-C resonant circuit depending on the impedance characteristics at the notched frequency [37]. From the imaginary part of the simulated impedance graph of Fig. 9(b), it can be seen that for the notch bands at 4.95 GHz, the imaginary component has a high value of resistance, showing a similar behavior of a parallel RLC circuit. Fig. 10 represents the equivalent circuit of the proposed UWB MIMO fractal antenna.

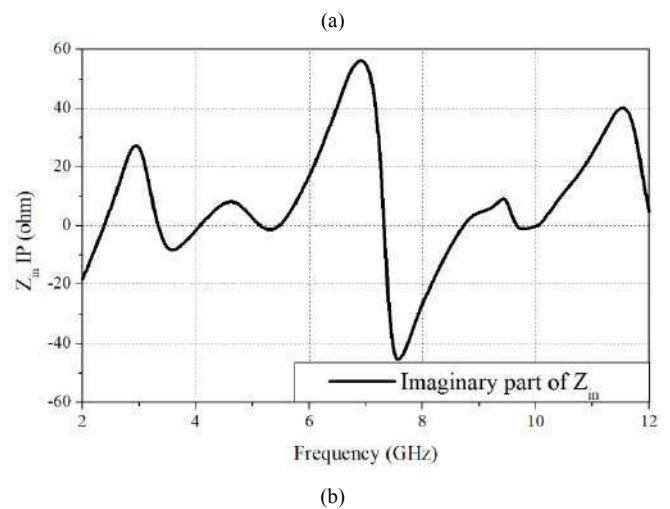
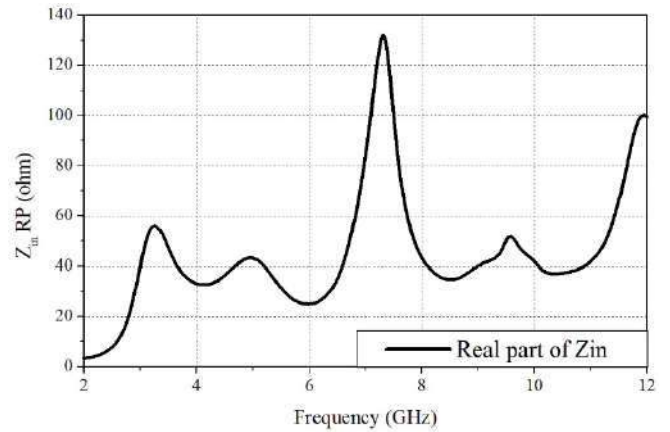


Fig. 9 (a) Real part and (b) Imaginary part of input impedance of the antenna

The parameters of the resistors, capacitors, and inductors in the equivalent circuit are as shown in Table. 2 and are obtained using foster canonical forms. The parallel RLC network acts as a bandpass filter, thus creating a resonance and the series RLC network acts as a band reject filter, thus rejecting the required frequency. A combination of the series RLC network and the parallel RLC network gives the desired UWB.

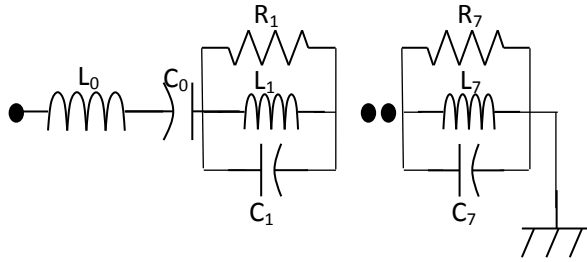


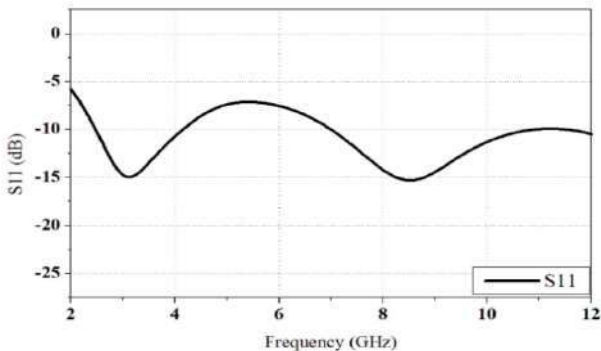
Fig. 10 Equivalent circuit of the antenna

Frequency (GHz)		3.26	4.95	6.74	7.32	9.59
R _n (Ω)		55.95	43.15	52.23	131.81	51.63
L _n (nH)	0.42	0.27	0.31	0.13	51.28	0.027
C _n (pF)	1.32	8.82	7.86	4.21	9.22	0.10

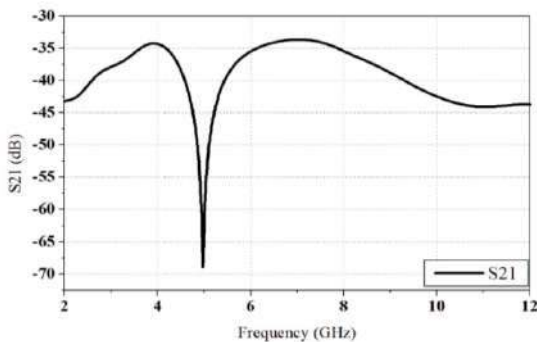
Table 2: Element values of the equivalent circuit

b. Simulated results

The simulated results show a bandwidth from 2.8 GHz to 10.4 GHz for S₁₁<-10 dB as shown in Fig. 11(a) Along with impedance matching, a mutual coupling less than -15 dB is obtained as represented in Fig. 11(b). The performance of the antenna is good with -10 dB impedance matching and high isolation.

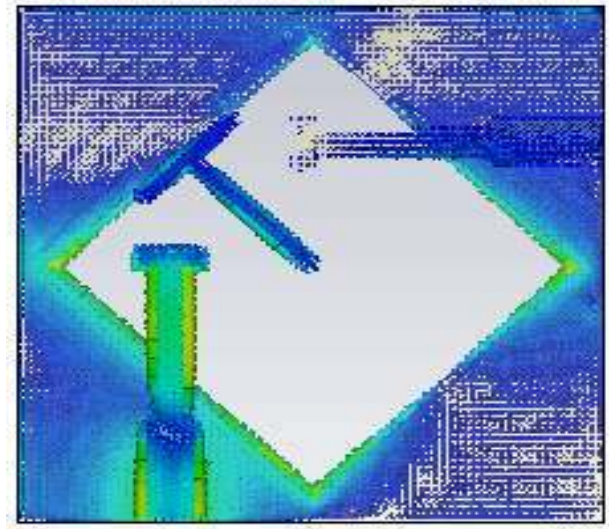


(a)

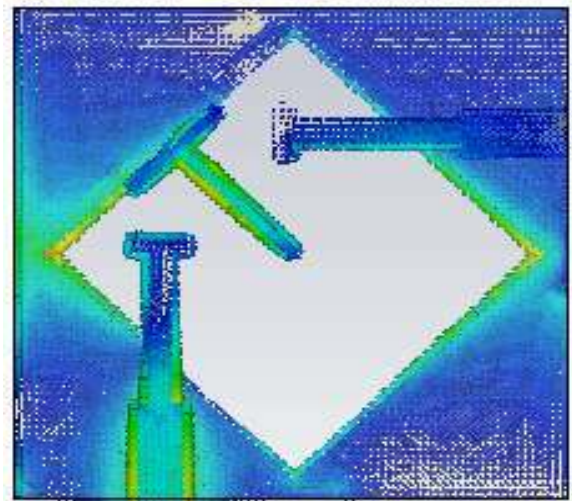


(b)

Fig. 11 (a) S₁₁ of parasitic element (b) S₂₁ of parasitic element



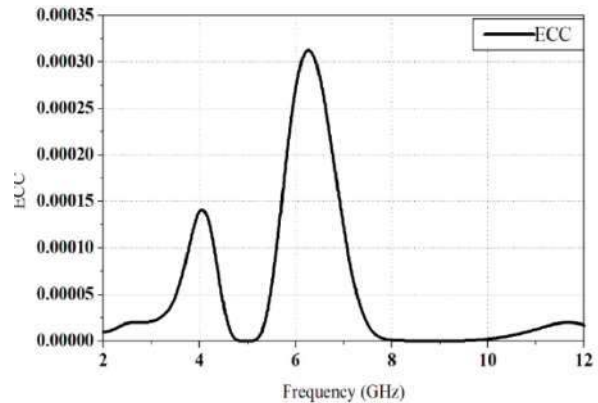
(a)



(b)

Fig.12 Surface current distribution at (a) 6 GHz and at (b) 7.5 GHz of the antenna

The mutual coupling obtained is less than -34 dB as represented in Fig. 11(b) in the required band of operation. It ensures that the above MIMO antenna is suitable for MIMO operations across the UWB band. There are two decoupling mechanisms used in the above antenna. The orthogonal polarization reduces the coupling, and the T-shaped parasitic strip further reduces the coupling and thereby improves the isolation between the antenna elements. The isolation obtained is very high.



(a)

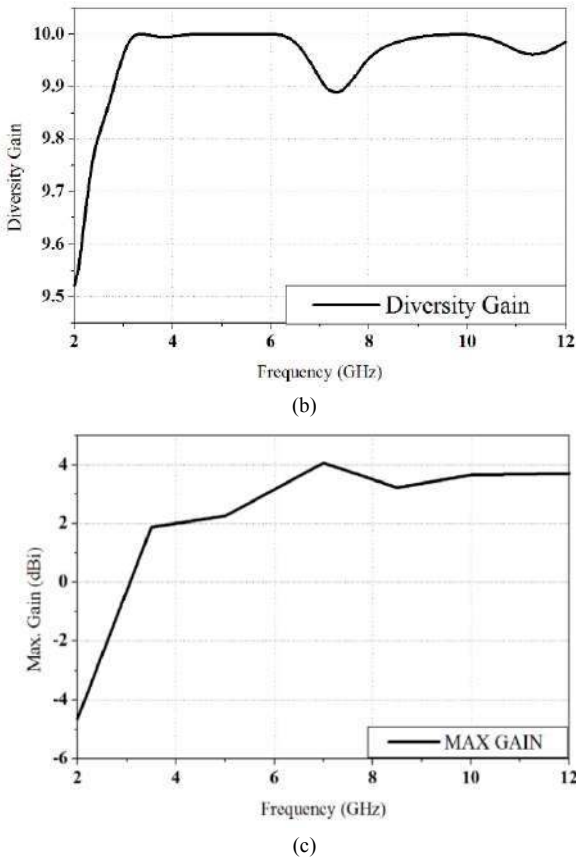


Fig.13 (a) Envelope Correlation Coefficient (b) diversity gain and (c) Maximum gain of the PE antenna

The isolation between the antenna elements can be analyzed using the surface current distribution. With a total length of 15.6 mm, the strip can excite a half wavelength resonant mode at 5 GHz. The antenna elements are placed orthogonally and this enhances the isolation between the antenna elements when compared to the antenna elements being placed symmetrically. From the surface current distributions as represented in Fig. 8(a), at 5 GHz, by adopting the parasitic structure, larger surface current is induced along the strip and an additional coupling path is created between the additional elements through the strip. The current that get coupled with the right antenna element decreases substantially with little effect on the impedance matching [9]. In Fig. 12(b), at 7.5 GHz the T shaped parasitic strip creates an opposite coupling and thus cancels the coupling from the antenna element 2.

The envelope correlation coefficient measures the correlation between the antenna elements. The ECC should be less than 0.5 to obtain good diversity performance [9]. The ECC obtained is near zero as represented in Fig. 13(a) and the diversity gain as shown in Fig. 13(b) is nearly equal to 10 dB throughout the UWB. It dips to 9.9 dB in the 6.2 to 8 GHz band. The ECC increases in the band reject frequency band and it is low at the other frequencies in the UWB. An antenna element with high isolation and with low correlation coefficient gives very good MIMO performance. The maximum gain of the MIMO antenna is 4 dBi as seen in Fig. 13(c) in the UWB frequency range.

VI. DECOUPLING NETWORK

The decoupling network gives a negative coupling which cancels the coupling due to the excited antenna on the adjacent antenna element thereby reducing the coupling

between the antenna elements. The coupling is mainly caused due to the space waves and surface waves. Extra power dissipation takes place between the antenna elements because of parasitic resistance whose presence cannot be avoided. Due to this, operations in the high frequency may not be suitable. The decoupling network complicates the structure of the antenna. But there is a number of MIMO antennas that utilizes decoupling network to increase the isolation between the antenna elements. In [10], a MIMO antenna utilizes a lumped network which consists of shunt and series elements. They are analytically designed using the even-mode analysis. The matching conditions of the even-odd modes are dealt with independently in the proposed decoupling network. This helps in achieving high isolation and good impedance matching for the MIMO antenna

But, a new decoupling structure that uses a floating parasitic digitated decoupling structure is proposed in [11]. It consists of a modified patch antenna with arced feeding section. The floating parasitic digitated decoupling structure was placed at the center of the ground. The decoupling structure is made up vertical stubs that are unequal in length and attached to a horizontal conducting strip. The antenna is as shown in Fig. 14. The dimensions of the antenna are $33 \times 45.5 \text{ mm}^2$. The height of the substrate is 1.524 mm and it is designed on Roger RO4003 having a dielectric constant of 3.55 and loss tangent 0.002.

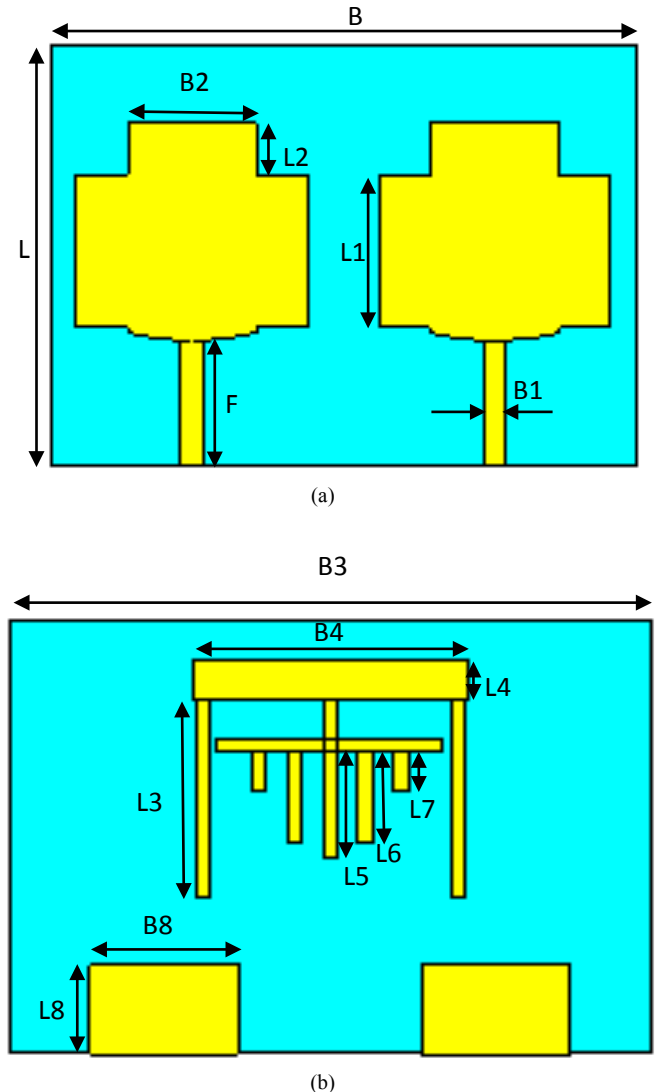


Fig.14 (a) top and (b) bottom layer of the antenna [11]

L	B	L1	L2	B1	B2	F	B3	B4
33	45.5	12	4	1.7	10	9.9	45.5	19.5
L3	L4	L5	L6	L7	L8	B8		
15	3	8	7	3	6	10.5		

a. Equivalent circuit of the antenna

The real part of the input impedance of S11 of the UWB MIMO antenna is shown in Fig. 15. From the real part of the input impedance of S11 from Fig. 15, it can be seen that the resonant peaks (parallel resonant modes) are at 4.72 GHz, 5.53 GHz, 6.02 GHz and at 9.55 GHz in the UWB and each frequency is represented as a parallel RLC circuit connected in series. The equivalent circuit of the antenna is as shown in Fig. 16.

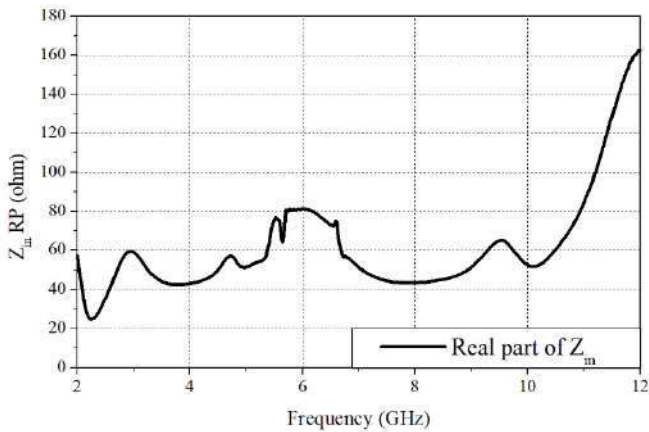


Fig. 15 The input impedance (real part) of the antenna

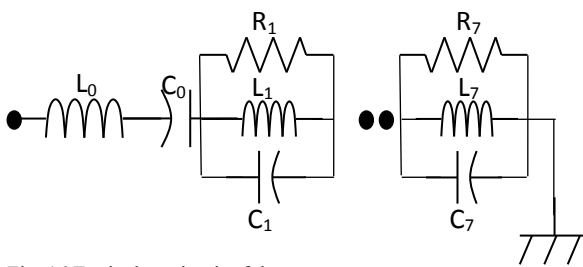


Fig. 16 Equivalent circuit of the antenna

Frequency (GHz)		4.72	5.53	6.02	9.55
R _n (Ω)		57.18	76.49	80.88	64.87
L _n (nH)	0.57	0.18	0.48	0.07	0.52
C _n (pF)	2.34	6.18	1.72	9.62	53.11

Table 3: Element values of the equivalent circuit

The parameters of the resistors, capacitors, and inductors in the equivalent circuit are as shown in Table. 3 and are obtained using foster canonical forms. The parallel RLC network acts as a bandpass filter, thus creating a resonance. A combination of the parallel RLC network and gives the desired UWB.

b. Simulation results

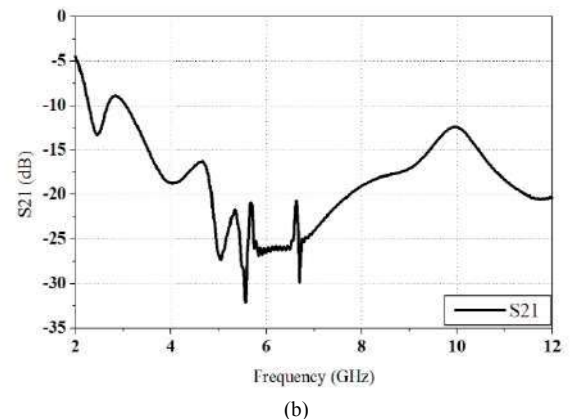
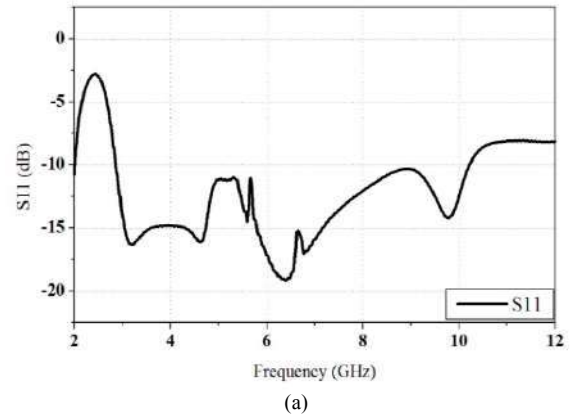


Fig.17 (a) S11 and (b) S21 of the antenna

The antenna resonates in the 3.1 – 10.6 GHz ultra-wideband frequency range as shown in Fig. 17 (a) with a S11 <-10dB in the desired frequency range. The isolation obtained is less than -15 dB as shown in Fig.17 (b) in the lower and upper-frequency bands and less than -20 dB in the middle frequency bands. The strips are arranged in the form of digits, the strips and slots formed in between them act as resonant elements for different frequencies and they help in improving isolation by adding multiple resonances in radiating band [11].

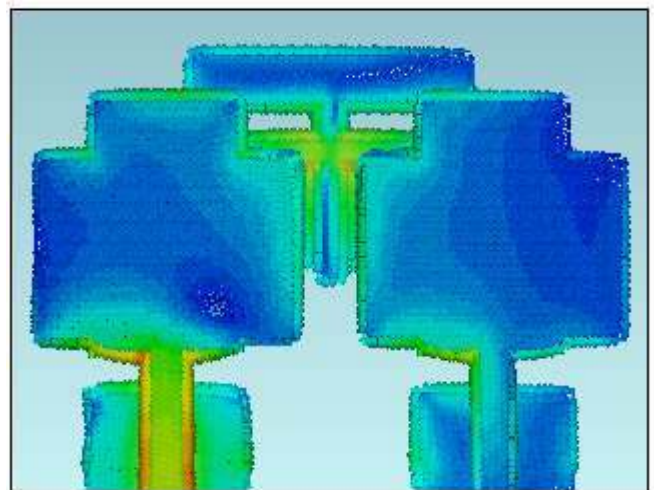


Fig.18 Surface current distribution of the antenna

From the surface current distribution in Fig. 18 at 6.5 GHz it is seen that the current is mainly concentrated in the decoupling structure. The decoupling structure acts as a bandgap structure and band reject filter and suppresses the surface currents in the stop band gaps of the filter and thus reduces the coupling between the antenna elements.

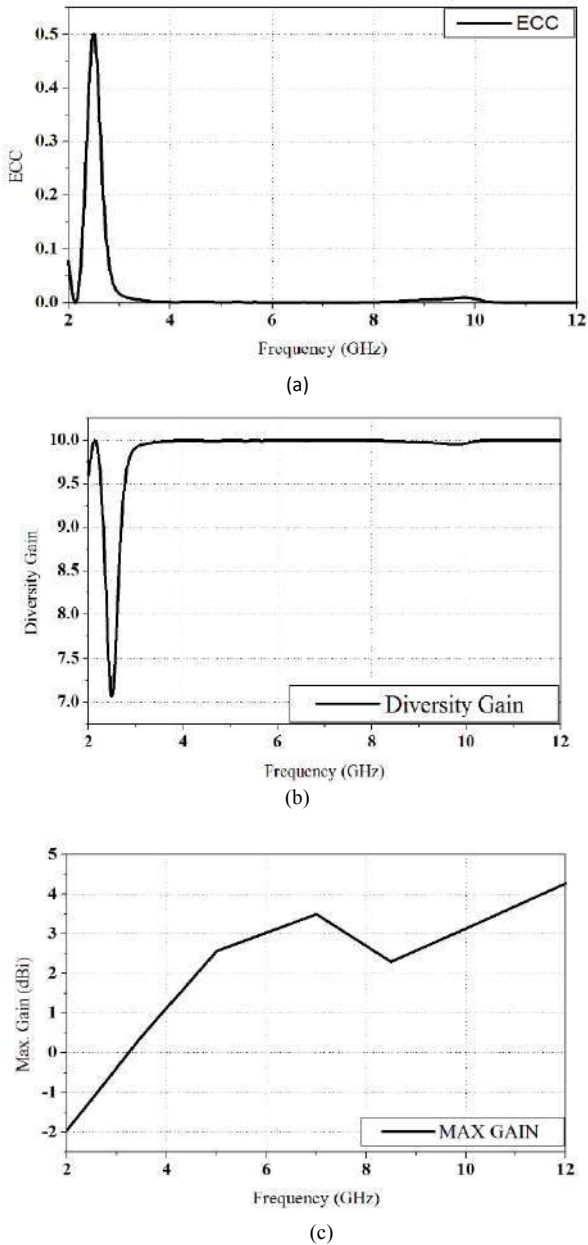


Fig.19 (a) ECC of the antenna (b) Diversity Gain of the antenna and (c) Maximum gain of the antenna

The envelope correlation coefficient as shown in Fig.19 (a) in the desired frequency range is nearly equal to zero and the diversity gain as shown in Fig. 19(b) is nearly equal to 10 dB in the band of interest from which it can be inferred that the antenna elements are nearly uncorrelated and they show good diversity performance [11]. The maximum Gain as shown in Fig.19 (c) obtained is 4 dBi in the UWB frequency range.

VII. DEFECTED GROUND STRUCTURES

A presence of a defect in the ground is represented as a defected ground structure (DGS). The defect induces inductance and capacitances, thereby acting as a band stop filter. The very first DGS is the dumbbell-shaped defect

created in the ground plane which was published in the year 1999. The shape and the dimensions of the defect disturb the current distribution in the ground plane and it spreads the electromagnetic waves in the substrate. As the defect produces inductances and capacitances, a band reject property is obtained, thereby suppressing the surface currents which decreases the coupling in multi-decibels. Careful tuning of the dimensions of the DGS reduces the surface currents. It enables bandwidth recovery and reduces the correlation between the antenna elements. The cross-polarization level of the radiating modes is effectively suppressed by DGS. It reduces the coupling in both the E plane and in the H plane. The high back radiation induces a current which is significantly reduced by using DGS. The main disadvantage of DGS is that it increases the effective space used.

In [12], a dual element triangular monopole is proposed. The isolation between the antenna elements is reduced by using a tree-like structure which behaves as a defected ground structure. Isolation is obtained due to two mechanisms. Firstly, through the tree-like structure, an isolation greater than 20 dB is obtained. Wideband isolation is obtained with the tree-like structure mainly due to two mechanisms, the first reason is that the branch 1 can be viewed as a reflector and the reflector separates the radiation patterns of the two antenna elements which reduces the mutual coupling. Increasing the number of branches further reduces the coupling between the antenna elements as it produces a number of resonances and these resonances reduce the coupling at that frequency. An L-shaped slot is utilized to increase the impedance bandwidth. The ECC obtained is less than 0.01.

In [13], the proposed antenna consists of eight antenna elements with each element consists of annular ring slots. For enhancing the isolation, frequency selective surfaces which are a closed loop in dimensions are introduced. Amongst few of the element isolation is also enhanced by introducing a quad strip which is connected to a circular arc. These decoupling structures introduces an isolation of more than 20 dB in the desired UWB band. A clamp like structure is introduced to improve the bandwidth. A defected ground structure is introduced but it improves the isolation in the higher bands only and not in the lower bands of operation. The size of the antenna is very large and it cannot be used for portable devices and mobile devices. The ECC obtained is very low for the UWB MIMO antenna.

Various defected ground structures like slots, stubs, and strips are introduced between the antenna elements to improve the isolation. Decoupling structures acts as an isolator between the antenna elements.

a. Introducing slots

Slots are introduced in between the antenna elements to improve the isolation. In [14], a MIMO antenna is proposed for portable ultra-wideband applications with a compact size of 22x36 mm². To improve the isolation between the input ports, a defect is created in the ground plane which consists of a long slot which is cut vertically. A T shaped stub in the ground plane acts as a defected ground plane and a slot cut on this stub suppresses the mutual coupling. The introduction of the ground slot improves the isolation from -12 dB to below -15 dB which satisfies the conditions for isolation. In [15], a compact MIMO antenna which consists

of a quasi-self-complementary antenna (QSCA) element and an inverted T defect in the ground plane is proposed.

The QSCA elements are perfect representations of each other where the antenna is having a conducting patch which is half-circular in shape on one side of the substrate and on the other side, a slot along with the complement of the half circular shape is introduced. In the ground plane, two rectangular slots are symmetrically cut in between the antenna elements, in order to decrease the mutual coupling. The slots also increase the impedance bandwidth. From the current distribution, it can be seen that the current is concentrated at the edges of the antenna elements and the current is also coupled from one antenna element to the other but with the introduction of rectangular slots, the amount of current coupled is reduced. The isolation obtained is greater than 15 dB with an ECC less than 0.1.

In [16], one of the antennas, a monopole, has been modified into a crescent shape and the other antenna is a modified slot antenna and the combination of these two reduces the coupling between the antenna elements. The impact of the different patterns and polarizations is used to enlarge the bandwidth of the antenna. Isolation is improved between the antenna elements because of the presence of the slot. The antenna exploits the slots which are formed due to the edges which are closely spaced to increase the isolation at the lower frequencies. Angle diversity and polarization diversity are also exploited to improve the isolation. The isolation obtained is greater than 20 dB and the ECC obtained is less than 0.1.

In [17], the proposed antenna comprises of two L-shaped slot antennas and a narrow slot is etched in the ground plane. The antenna elements are placed perpendicular to each other to exploit orthogonal polarization, and to enhance the isolation and the slots which resonate at $\lambda/4$ wavelength and slots are introduced to reduce the mutual coupling and to improve the isolation. From the current distribution, it is seen that the slots block the current flowing between the antenna elements and thus the coupling current is reduced. The isolation obtained is greater than 20 dB and the ECC obtained is less than 0.005. In [18], an antenna which comprises of a rectangular patch with an L-shaped slot is proposed. The elements are placed perpendicular to each other to enhance the isolation, and in the ground plane, a rectangular slot is etched to improve the isolation. The slot forces the current to be concentrated near it and it resonates at the $\lambda/4$ wavelength. This mechanism reduces the coupling between the antenna elements. The introduction of the slot improves the isolation by 10 dB. In [19], a dual polarized slot antenna which consists of a square ring having identical arms and stepped rectangular arms is proposed. The slot behaves as a stepped impedance resonator (SIR) and its profile is tapered. The adjacent arms of the ring are helpful in exploiting orthogonal polarization. Tilted stubs which consist of metallic stubs and slot stubs are attached to the corners of the arms of the stub where the metallic stubs reduce the coupling by blocking the spread of the electric current into the neighbor arms and the slot stubs concentrate the current around it. The isolation is enhanced by inserting stubs. The isolation obtained is greater than 20 dB and the ECC obtained is greater than 0.005.

b. Introducing stubs

In [20], an eye-shaped slotted circular monopole antenna is adopted as the elementary antenna element for the proposed MIMO antenna. To improve the isolation, a T-shaped stub is introduced in the ground plane. A T-shaped stub is extruded in the ground plane to improve isolation. This changes the surface current distribution, and thus improves isolation. The isolation obtained is greater than 20 dB and the ECC obtained is less than 0.1. In [21], the antenna consists of two monopoles which are rectangular in shape and to improve the isolation between the antenna elements a ground stub which is having a simple stepped structure is introduced. The simply stepped stub reflects the radiation pattern of the antenna elements, and it resonates due to the radiating structure, thereby leading to strong current distribution on the stub. This improves the isolation as very less current is coupled to the neighboring antenna element. The isolation obtained is greater than 21 dB and the ECC obtained is less than 0.005. But the impedance matching is not present in the higher band from 8.2 GHz onwards.

In [22], a UWB-MIMO antenna is proposed which is fed by an asymmetric coplanar strip (ACS). It contains of a shared quarter circular radiator and the two ports of the radiator are fed by ACS. The introduction of an I-shaped slot in the antenna element and a rectangular patch in the ground, isolation is enhanced. To improve the isolation between the antenna elements, a U-shaped slot is also introduced in the ground plane of the antenna. The isolation obtained is greater than 15 dB. But the radiation pattern is not omnidirectional in all directions as it has been concluded. In [23], the antennas consist of two rectangular monopoles placed perpendicular to each other to enhance the isolation. To enhance the isolation further, two long protruding ground stubs are added to the ground plane. The isolation obtained is greater than 15 dB and the ECC obtained is less than 0.2. In [24], Koch fractal geometry is used where the antenna elements are octagonal in shape and the self-similar and self-filling properties of the above geometry are utilized in the antenna elements. Placing these Koch fractal geometry antenna elements orthogonal to each other improves the isolation. To further improve the isolation between the antenna elements, stubs in the ground plane are introduced. Band notching is obtained by introducing a C-shaped slot in the antenna element itself.

In [25], antenna elements having a staircase structure are placed orthogonally. Orthogonal polarization is exploited to improve the isolation. A $\lambda/4$ wavelength circular slot is created in the ground plane and it increases the length of the coupling current and thereby improves the isolation. A rectangular stub is placed which blocks the current flowing between the two antenna elements and thus ensures high isolation

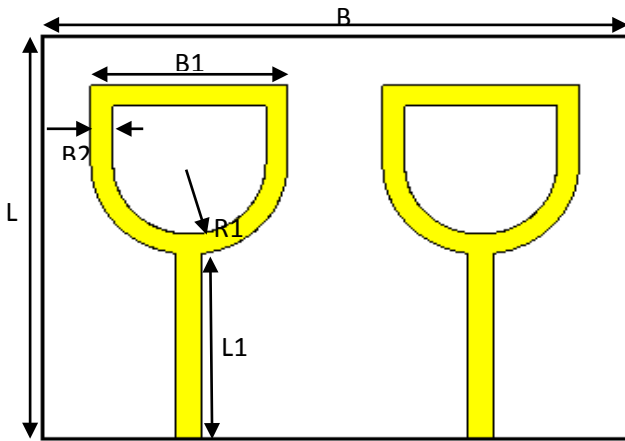
c. Introducing strips

In [26], a monopole antenna which consists of two identical co-planar waveguide strips ending in a U-shaped stub and an open annular slot in the ground plane is proposed. The dual polarization is achieved by orthogonally placing the feeding structure which consists of the coplanar waveguide and a U-shaped slot. High isolation is achieved by introducing a strip diagonally in the ground plane. The coupling between the open-annulus ground and the feeding structure is improved. The impedance bandwidth is also

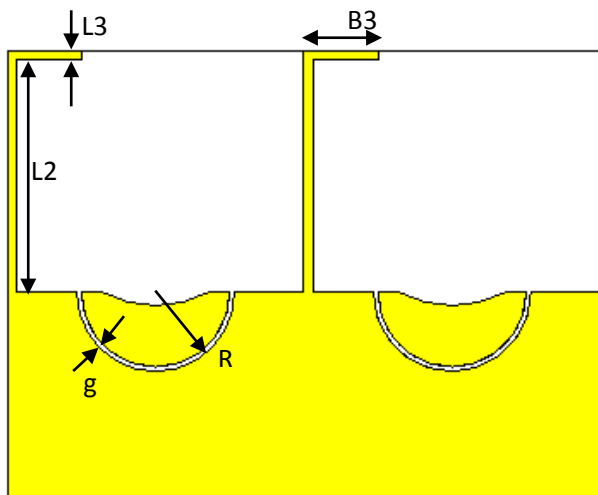
widened by the combination of several dominant resonances produced by the open annular ground. By loading the arch-shaped slot resonators which are present in the feeding structure, band notch in the 4.75-6.12 GHz frequency band is achieved. The main disadvantage of this antenna structure is its size. The isolation obtained is greater than 15 dB. In [27], the antenna elements are attached to the protruded ground parts, and the protruded ground parts are attached together by a strip to enhance the isolation. A $1/3 \lambda$ rectangular metal strip which acts as a loop having a 1λ loop path produces the notched band from 5.15 to 5.85 GHz band. A $1/4 \lambda$ slot in the antenna element is required to produce the notched band from 3.30 – 3.70 GHz. The isolation obtained is greater than 20 dB and the ECC obtained is less than 0.012.

In [28], a staircase shaped radiator with a metal strip at the bottom is proposed. The metal strip which behaves as a reflector reduces the coupling between the two antenna elements. The antenna elements are back to back configured and this enhances the isolation further. The isolation obtained is greater than 20 dB and the ECC obtained is less than 0.16.

In [29], a hybrid antenna is proposed which consists of a half circular ring and a half square ring. A defected ground structure is introduced in the ground plane which is used to enhance the isolation between the antenna elements. This also improves the impedance bandwidth. A stub is introduced in the ground plane to further enhance the isolation.



(a)



(b)

Fig.20 the (a) top and (b) bottom layer of the antenna [29]

L	B	B1	B2	R1	L1	L2	L3	B3
24	35	9.4	1.2	4.2	11	5	0.5	4
g	R							
0.25	4							

The antenna is as shown in Fig.20. The dimensions of the antenna are $24 \times 18 \text{ mm}^2$ and the height of the substrate is 0.8 mm. The antenna is designed on a thick FR4 substrate with has a dielectric constant of 4.3 and having a loss tangent of 0.02.

a. Equivalent Circuit

The real part of the input impedance of S_{11} of the UWB MIMO antenna is shown in Fig. 21. From the real part of the input impedance of S_{11} from Fig. 21, it can be seen that the resonant peaks (parallel resonant modes) are at 4.21 GHz, 6.83 GHz and at 7.96 GHz in the UWB and each frequency is represented as a parallel RLC circuit connected in series. The equivalent circuit of the antenna is given in Fig. 22.

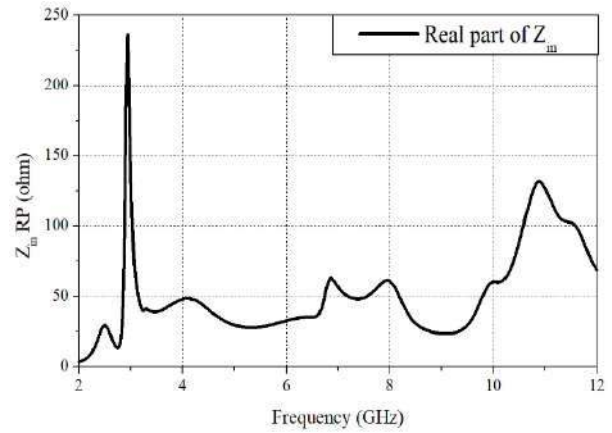


Fig. 21 Input impedance (Real part) of the antenna

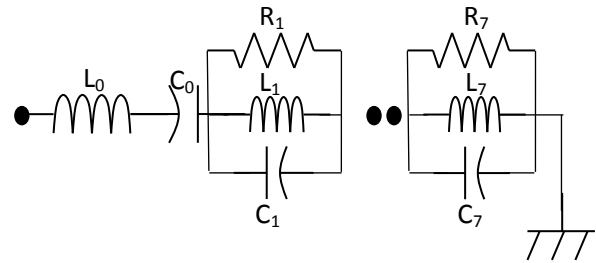


Fig. 22 Equivalent circuit of the antenna

Frequency (GHz)		4.21	6.83	7.96
R_n (Ω)		33.86	36.39	35.79
L_n (nH)	0.34	0.41	0.83	0.064
C_n (pF)	1.56	3.52	65.12	6.23

Table 4: Element values of the equivalent circuit

The parameters of the resistors, capacitors, and inductors in the equivalent circuit are as shown in Table. 4 and are obtained using foster canonical forms. The parallel RLC network acts as a bandpass filter, thus creating a resonance. A combination of the parallel RLC network gives the desired UWB.

b. Simulated Results

The MIMO antenna with the defected ground structure resonates in the frequency range from 2 GHz to 12 GHz as shown in Fig. 23 (a) with $S_{11} < -10$ dB. The isolation obtained as shown in Fig. 23 (b) is greater than 15 dB in the lower band and greater than 10 dB in the higher band of operation.

The isolation can be analyzed by using surface current distribution. A partial ground plane is introduced which enhances the bandwidth of the antenna. A semicircular ring is etched out from the ground which acts as a defected ground structure. The defect in the ground increases the current path. A stub is also inserted in the ground plane to improve the isolation between the antenna elements. The surface current distribution at port_1 at 5.5 GHz is as shown in Fig.24. The current is distributed in the antenna 1 and concentrated in the ring and the stub in the ground plane. The slit and stubs act as a band reject filter and suppress the surface currents in the antenna. The antenna element 2 is isolated from the antenna element 1 due to the presence of the defected ground structures which reduces the coupling between the antenna elements.

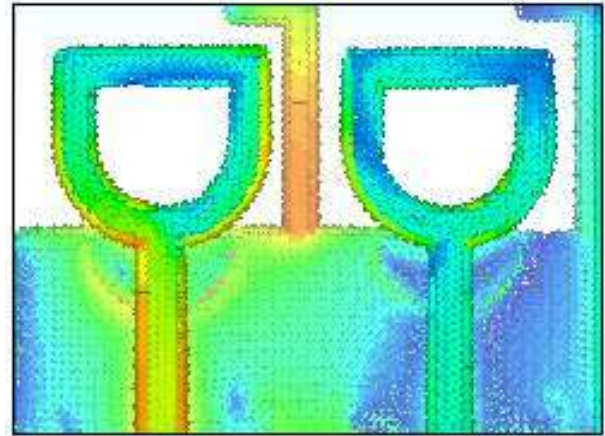
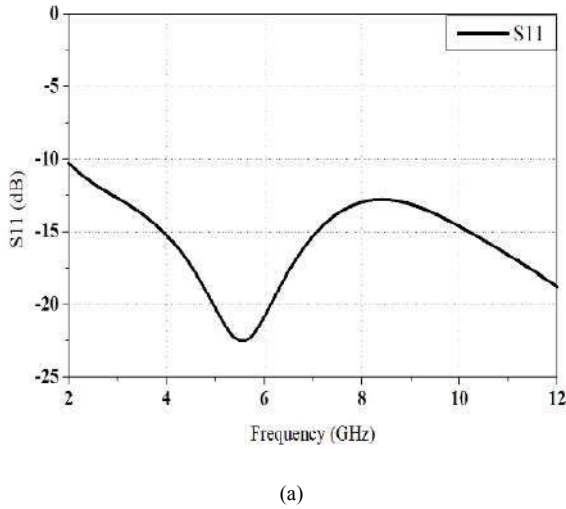
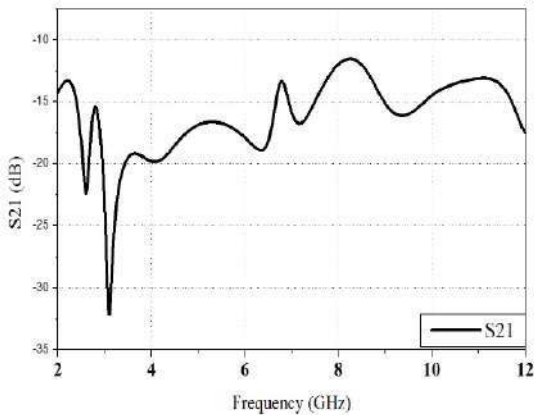


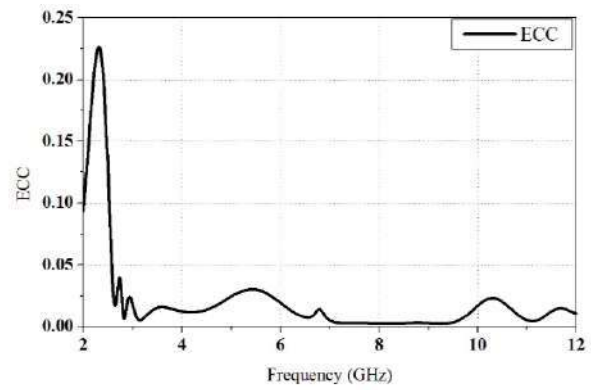
Fig.24 Surface current distribution of the antenna



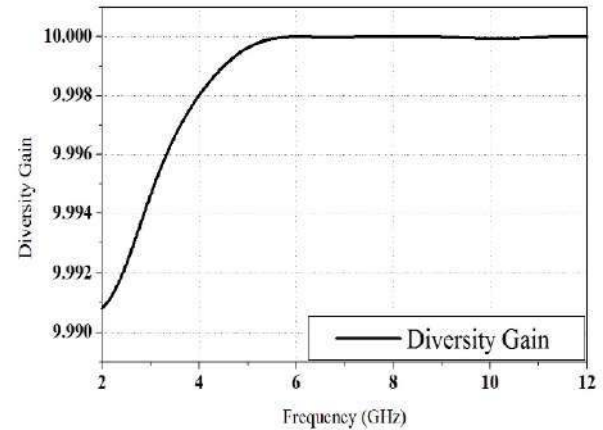
(a)



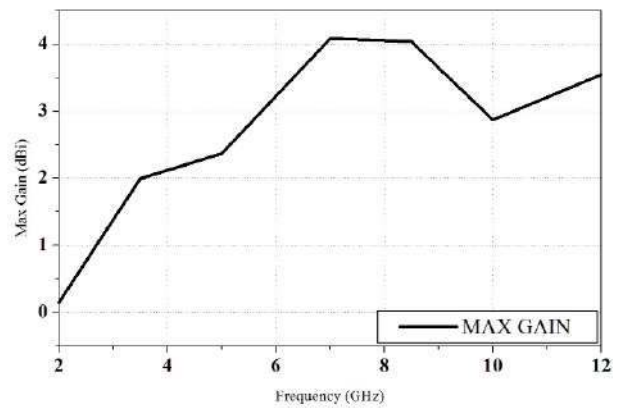
(b)



(a)



(b)



(c)

Fig.23 (a) S11 of the defected ground structure (b) S21 of the defected ground structure

Fig. 25 (a) ECC of the defected ground structure (b) Diversity gain of the defected ground structure (c) Maximum gain of the defected ground structure

The envelope correlation coefficient of the antenna is as shown in Fig.25 (a) is less than 0.025 and it is very much less than the required value of 0.5 and the diversity gain as shown in Fig. 25 (b) is nearly 10 dB above 4 dB and it varies from 9.94 to 10 dB from 3.1 dB it gives very good diversity performance in the band of interest. The maximum gain is as shown in Fig. 25 (c) of the antenna is 4 dBi.

In [38], a MIMO antenna that utilizes the defected ground structure technique is proposed as shown in Fig. 26. The dimensions of the MIMO antenna are 22x32 mm². The height of the substrate is 1.6 mm. The antenna is designed on an FR4 substrate with relative permittivity of 4.3 and having a loss tangent of 0.02.

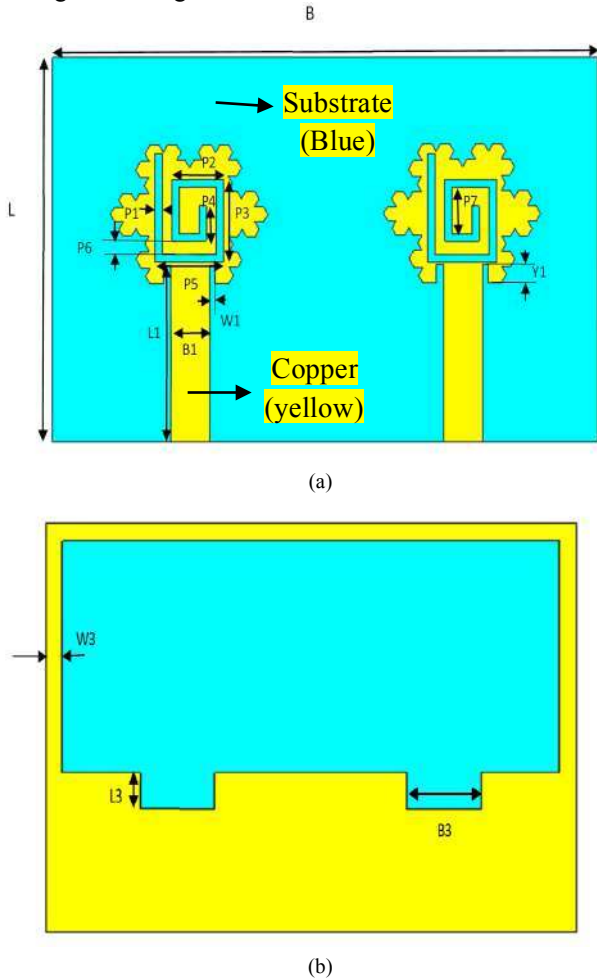


Fig. 26 (a) The top and (b) The bottom layer of the UWB-MIMO antenna [38]

c. Equivalent circuit of the antenna

The real part of the input impedance of S_{11} of the UWB MIMO antenna is shown in Fig. 27(a). From the real part of the input impedance of S_{11} from Fig. 27(a), it can be seen that the resonant peaks (parallel resonant modes) are at 3.5 GHz, 4.1 GHz, 5.3 GHz, 6.3 GHz, 8.2 GHz, 9.3 GHz and at 10.3 GHz in the UWB and each frequency is represented as a parallel RLC circuit connected in series. The equivalent circuit of the antenna is as shown in Fig. 28.

The parameters of the resistors, capacitors, and inductors in the equivalent circuit are as shown in Table. 5 and are obtained using foster canonical forms. The parallel

RLC network acts as a bandpass filter, thus creating a resonance and the series RLC network acts as a band reject filter, thus rejecting the required frequency. A combination of the series RLC network and the parallel RLC network gives the desired UWB.

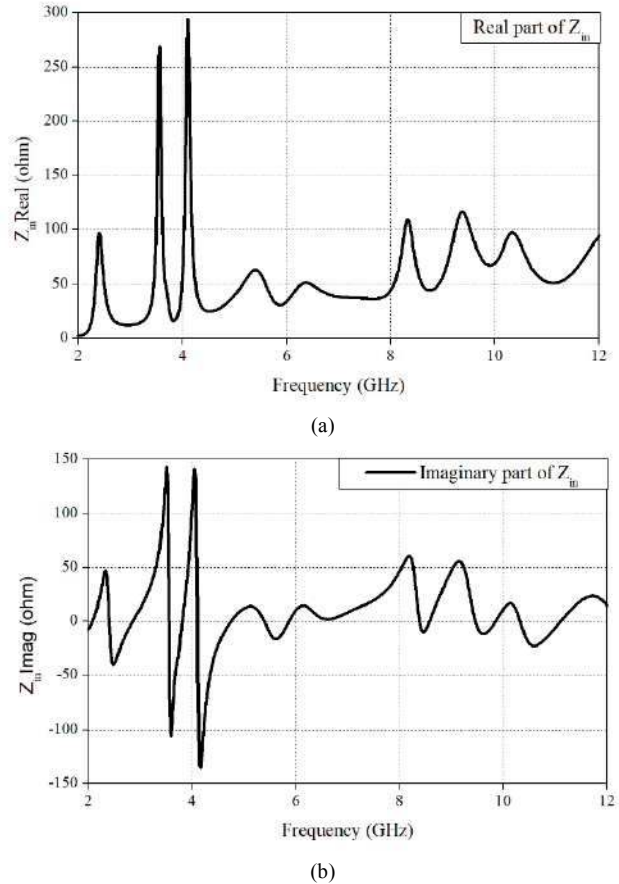


Fig. 27 (a) Real part and (b) Imaginary part of the input impedance of the antenna

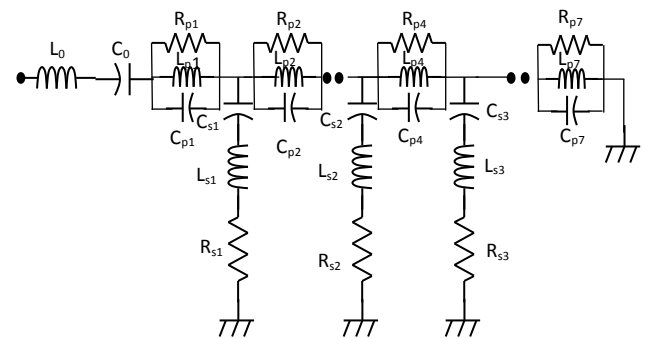


Fig. 28 Equivalent circuit of the antenna

Freq (GHz)		3.5	4.1	5.3	6.3	8.2
R _{pn} (Ω)		243.4	282.67	62.96	51.57	112.1
L _{pn} (nH)	0.63	0.497	1.165	6.33	7.438	9.293
C _{pn} (pF)	1.09	4.089	13.07	1.38	0.84	0.399
Freq (GHz)	9.3	10.3	Freq (GHz)	3.8	5.9	7.9
R _{pn} (Ω)	118.6	97.23	R _{sn} (Ω)	16.05	27.81	42.65

L_{pn} (nH)	6.734	4.152	L_{sn} (nH)	0.093	0.214	8.497
C_{pn} (pF)	0.431	2.679	C_{sn} (pF)	18.48	0.152	0.475

Table 5. Element values of the equivalent circuit

d. Simulated results

The antenna resonates in the 3.1 – 12 GHz with $S_{11} < -10\text{dB}$ as shown in Fig. 29 (a). The antenna rejects the C-band downlink frequency from 3.7 - 4 GHz, the C-band uplink frequency from 5.925 - 6.25 GHz and the satellite bands from 7.45 to 8.4 GHz. The band 7.45 - 7.55 GHz is used by the meteorological satellite service for the geostationary satellite services. The band 7.75 - 7.9 GHz is used by the meteorological satellite service for non-geostationary satellite services. The band 8.025 - 8.4 GHz is used by the Earth exploration satellites for geostationary satellite services. The isolation obtained is greater than 22 dB as shown in Fig. 29 (b) and it has good diversity performance.

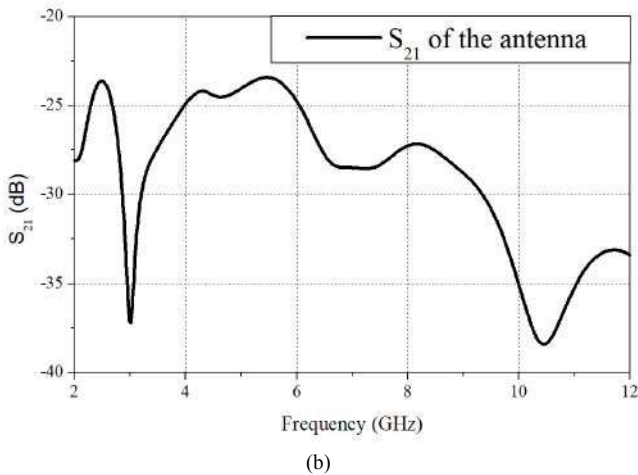
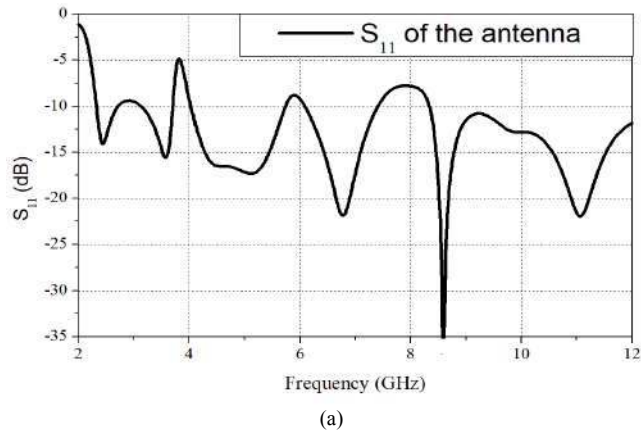


Fig. 29 (a) S_{11} and (b) S_{21} of the antenna

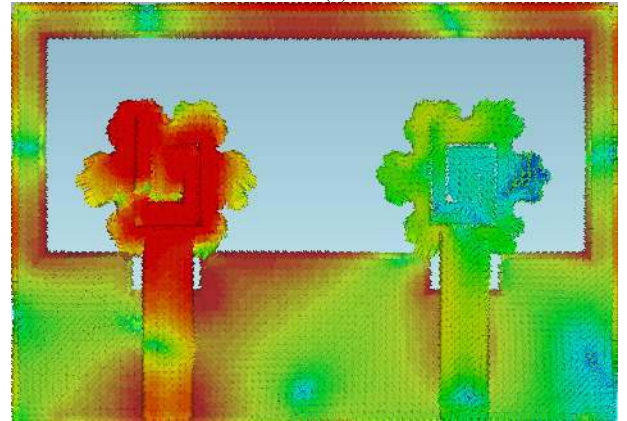
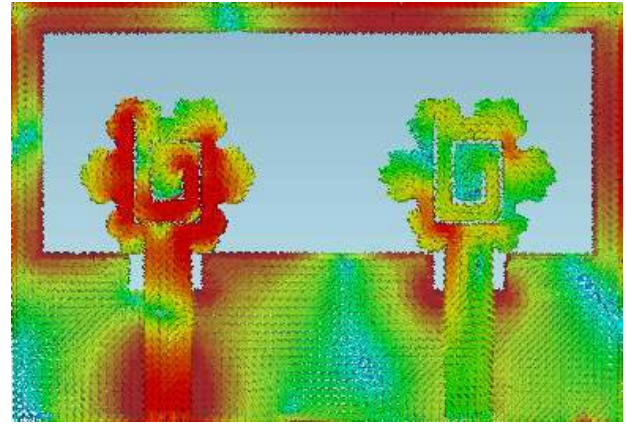
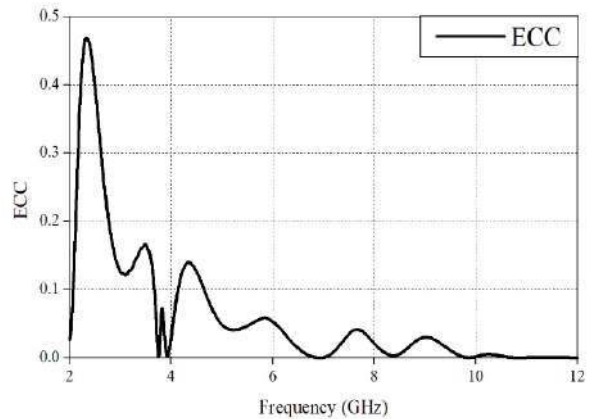
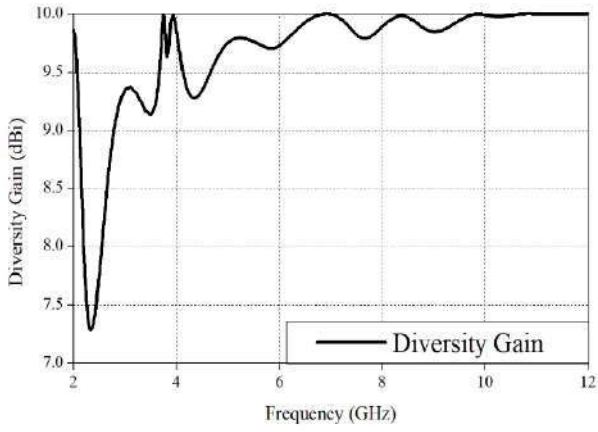


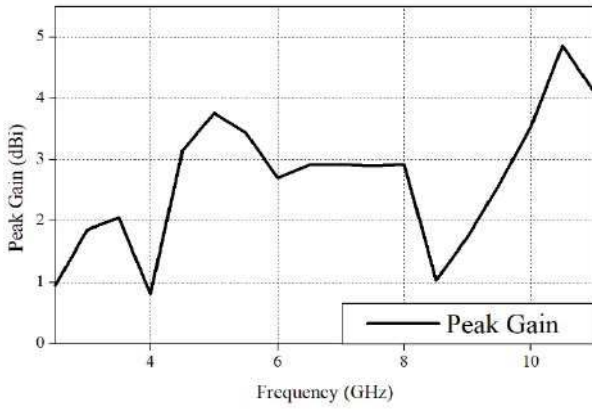
Fig. 30 Surface current distribution at (a) 3.6 GHz and at (b) 6.8 GHz

The isolation between the antenna elements can be analyzed using surface current distribution as shown in Fig. 30. To reduce the mutual coupling between the antenna elements, a ring structure is placed in the ground. The ring structure behaves as a defected ground structure and it reduces the mutual coupling between the antenna elements by behaving as a band reject filter [37]. The introduction of the partial ground, the defect in the ground and the ring structure reduces the coupling between the antenna elements.





(b)



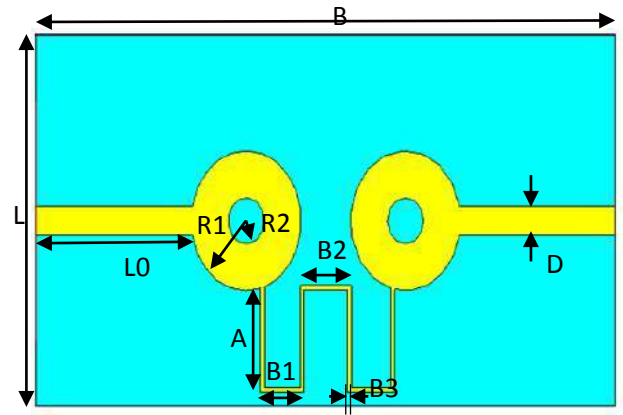
(c)

Fig.31 (a) ECC (b) Diversity gain and (c) Maximum gain of the antenna

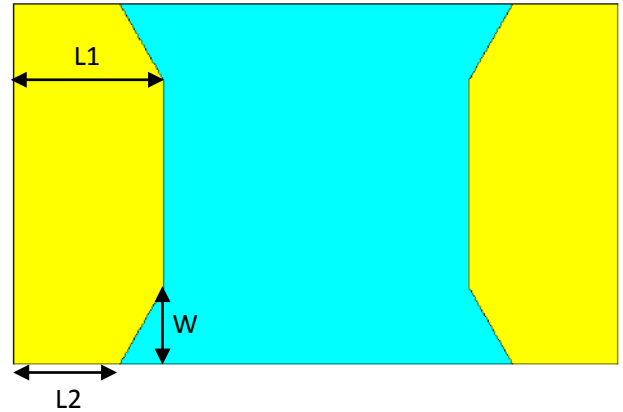
The ECC of the antenna using neutralization as shown in Fig. 31 (a) is less than 0.3. The ECC of the antenna increases at the band notches, thus rejecting the required bands. The diversity gain of the antenna is as shown in Fig.31 (b). It is greater than 9.25 dB and it shows that the antenna elements are uncorrelated in the band of interest. The antenna has good diversity performance [37]. The maximum gain is 5 dBi as shown in Fig. 31 (c).

VIII. NEUTRALIZATION LINE

In the neutralization line technique, the current of the exciting element is taken at a specific location, and an appropriate length of the neutralization line is selected and the phase is inverted, and to reduce the amount of coupled current the current that was inverted is fed to the adjacent antenna. With the antennas becoming more compact in space, neutralization line technique is the best technique as it requires less board space and there is no modification in the ground plane. The lack of a systematic approach to determine the location of the neutralization line makes this technique rely mostly on a try-and-error process. In [30], a MIMO antenna that utilizes the neutralization line technique to suppress the isolation between the antenna elements is proposed as shown in Fig. 32. The dimensions of the MIMO antenna are $40 \times 80 \text{ mm}^2$. The height of the substrate is 1.6 mm. The antenna is designed on an FR4 substrate with relative permittivity of 4.4 and having a loss tangent of 0.02.



(a)



(b)

Fig. 32 the (a) top and (b) bottom layer of the antenna [30]

L	B	L0	R1	R2	A1	B1
40	80	21.4	7.6	2.5	12	6.5
B2	B3	D	L1	L2	W	
7	0.5	3	19.8	14	8.5	

a. Equivalent Circuit

The real part of the input impedance of S_{11} of the UWB MIMO antenna is shown in Fig. 33. From the real part of the input impedance of S_{11} from Fig. 33, it can be seen that the resonant peaks (parallel resonant modes) are at 3.61 GHz, 4.21 GHz, 7.04 GHz and at 8.18 GHz in the UWB and each frequency is represented as a parallel RLC circuit connected in series.

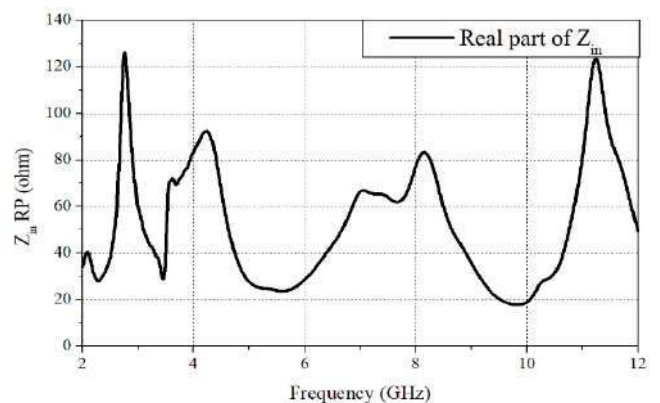


Fig.33 Input impedance (Real part) of the antenna

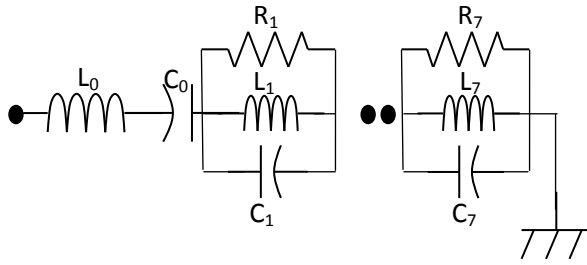


Fig. 34 Equivalent circuit of the antenna

The equivalent circuit of the antenna is as shown in Fig. 34. The parameters of the resistors, capacitors, and inductors in the equivalent circuit are as shown in Table. 6 and are obtained using foster canonical forms. The parallel RLC network acts as a bandpass filter, thus creating a resonance. A combination of the parallel RLC networks and gives the desired UWB.

Frequency (GHz)		3.61	4.21	7.04	8.18
R_n (Ω)		71.58	92.05	66.74	82.89
L_n (nH)	2.98	0.98	0.71	0.42	0.16
C_n (pF)	0.41	1.98	2.04	1.22	2.36

Table 6: Element values of the equivalent circuit

b. Simulated results

The antenna resonates in the 2.8 – 12 GHz with $S_{11} < -10$ dB as shown in Fig 35 (a). The isolation obtained is greater than 20 dB as shown in Fig. 35(b) in the band of interest and it has good diversity performance.

The surface current distribution of Fig. 36 shows that the inversion of phase takes place due to the neutralization line and the current with opposite phase is given to the neighboring antenna and hence the coupling is reduced between the antenna elements. Further improvement in isolation is obtained due to the triangular slot in the ground plane. In the upper-frequency band from 3.1 to 6.2 GHz the isolation obtained is greater than 20 dB and less than 25 dB and in the higher band, i.e., from 6.5 to 10.6 GHz, the isolation is greater than 26 dB. At 6.65 GHz, the isolation is highest having a value of 31.5 dB.

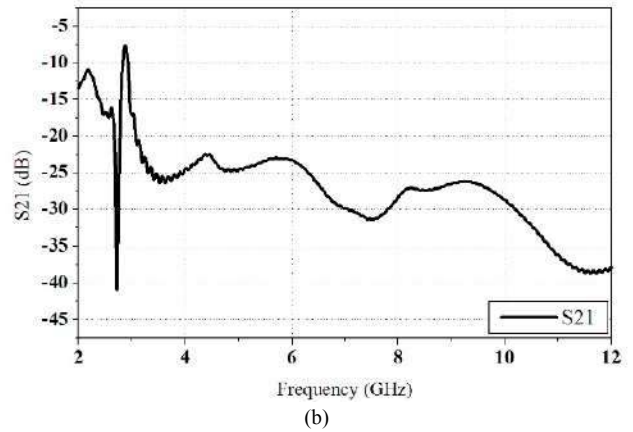


Fig.35 (a) S_{11} of antenna (b) S_{21} of the antenna

From the surface current distribution as shown in Fig. 36, it can be observed that at 8.5 GHz, the currents are concentrated at the edges of the patch. At 8.5 GHz, along with the neutralization line, there is a change of phase of 180° and the mutual coupling between the antenna elements is suppressed.

The ECC of the antenna using neutralization as shown in Fig. 37 (a) is nearly equal to 0 and the diversity gain as shown in Fig. 37 (b) is nearly equal to 10 dB and dips to 9.5 dB in the 3-4 GHz band and it shows that the antenna elements are uncorrelated in the band of interest. The maximum gain as shown in Fig. 37 (c) obtained is 4 dBi in the lower frequency band and 5 dBi in the upper frequency band.

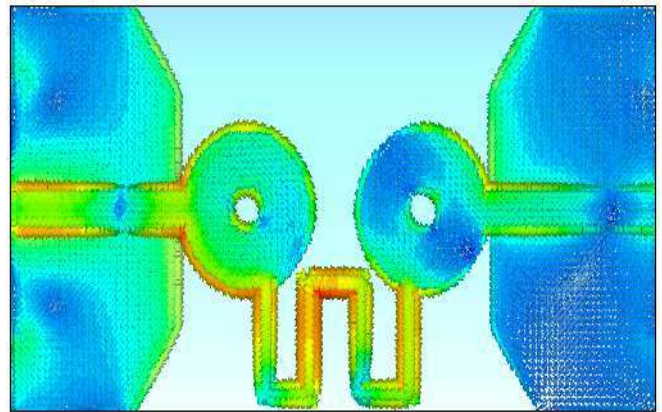
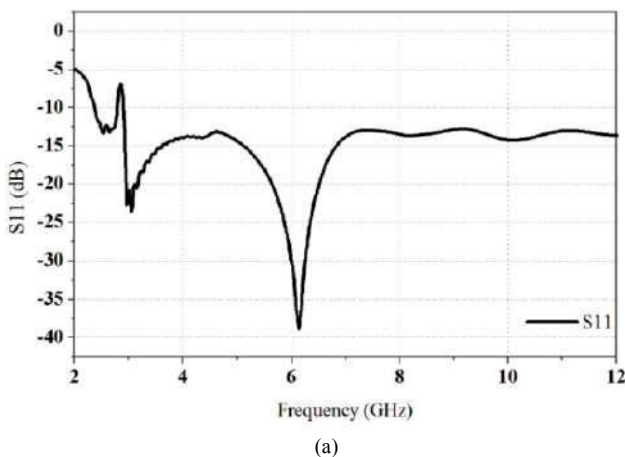
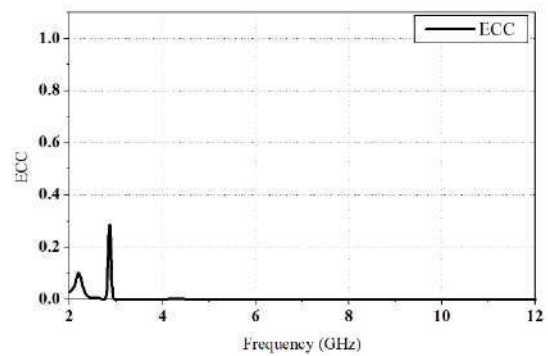


Fig.36 the surface current distribution at port_1 at 8.5 GHz of the antenna



(a)



(a)

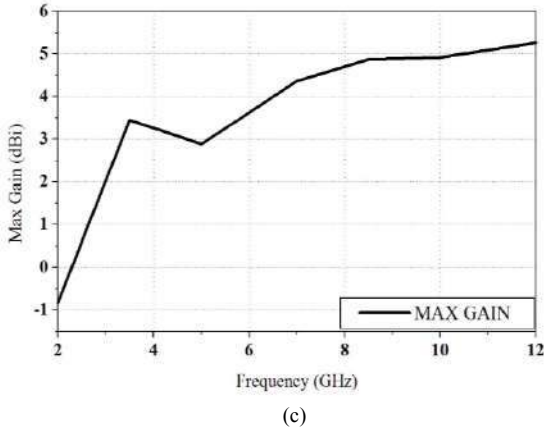
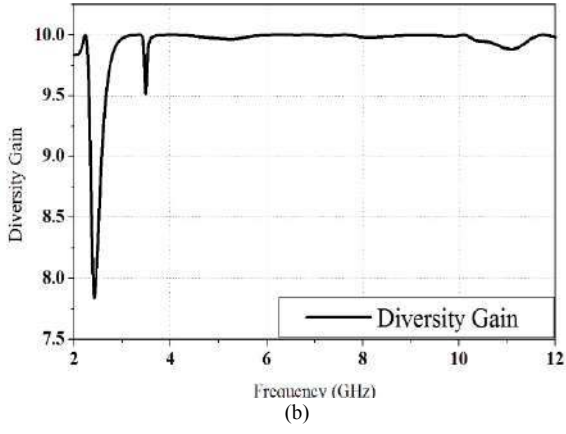


Fig.37 (a) ECC of the neutralization line (b) Diversity gain and (c) Maximum gain of the antenna

IX. METAMATERIALS

Metamaterials have the properties of either negative permittivity or permeability or a combination of both these properties. Metamaterials are classified as metamaterial-based antennas and metamaterial – inspired antennas. The antennas that utilize the metamaterial unit cells are known as metamaterial-inspired antennas. Metamaterial-based antennas are divided into two types, antennas that utilize negative permeability substrates i.e., ENG (ϵ -negative), that utilize negative permittivity substrates, MNG (μ -negative) or those which have both permeability and permittivity negative, DNG (double Negative) substrates. The metamaterial-inspired antennas are the split ring resonator (SRR), the complementary split ring resonator (CSRR) and the capacitively locked loops (CLL).

Metamaterials are introduced in MIMO antennas primarily to improve the isolation between the antenna elements as the metamaterials produce a band gap and these act as band stop filters and suppress the mutual coupling between the antenna elements. The widely used metamaterials are the SRR, CSRR and the CLL which are used to improve the isolation in a MIMO antenna. SRR is also used to obstruct the electromagnetic fields from the adjacent antenna element if the external magnetic field is having an angle of 90° to the resonator rings. It also acts as an insulator and reduces the coupling between the antenna elements. Here, an analytical expression for the resonant frequency of the single split ring resonator is derived. The split ring resonator used for this analysis is shown in Fig. 38 (a). The parameters used are the inner radius of the ring, R , the thickness, w , the height, h , and the gap width, g . The

inductance, L , and the capacitance, C , is used to characterize the sub-wavelength SRR.

The frequency of the antenna is calculated as

$$f_0 = \frac{1}{2\pi\sqrt{LC}} \quad [16]$$

where the inductance is equated to a closed ring, the inductance is given by

$$L = \mu_0 R_m \left(\ln \frac{8R_m}{h+w} - 0.5 \right) \quad [17]$$

where μ_0 is the permeability of free space and R_m is the mean radius of the ring $R_m = R + w/2$

To determine the capacitance, two capacitances are considered, the gap and the surface capacitances. The gap capacitance is generated by the charges in the gap and a parallel plate capacitance is formed due to the gap

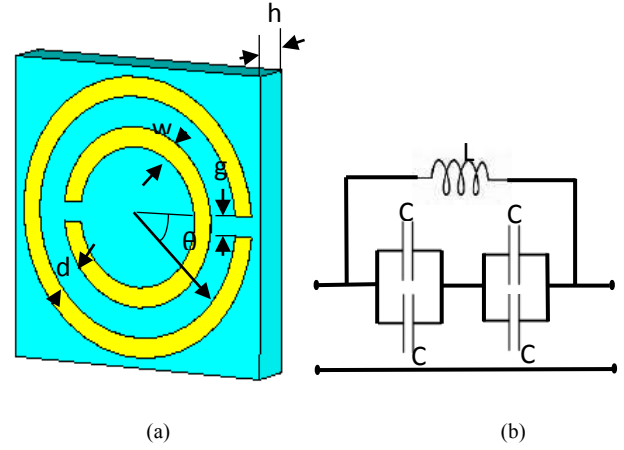


Fig.38 (a) The geometry of the ring under analysis (b) Two port equivalent network of the SRR Unit

$$C_{gap} = \epsilon_0 \left[\frac{wh}{g} + \frac{2\pi h}{\ln \left(\frac{2.4h}{w} \right)} \right] \quad [16]$$

The surface capacitance is generated by the charges that are present on the surface of the ring. The surface charge density, σ and the voltage V are calculated as

$$\sigma = \frac{\epsilon_0 V_0}{2\pi R} \cot \frac{\theta}{2} \quad [18]$$

$$V = \frac{C}{\pi} (\pi - \theta) \quad [19]$$

where V_0 is the applied voltage to the gap and the θ is the angle as shown in Fig.22(a) above. The surface capacitance is given by

$$C_{surf} = \int_{\theta_g}^{\pi} \frac{\sigma R d\theta}{V} = \epsilon_0 h \int_{\theta_g}^{\pi} \frac{\cot \frac{\theta}{2}}{\pi - \theta} d\theta \approx \frac{2\epsilon_0 h}{\pi} \ln \frac{4R}{g} \quad [20]$$

where

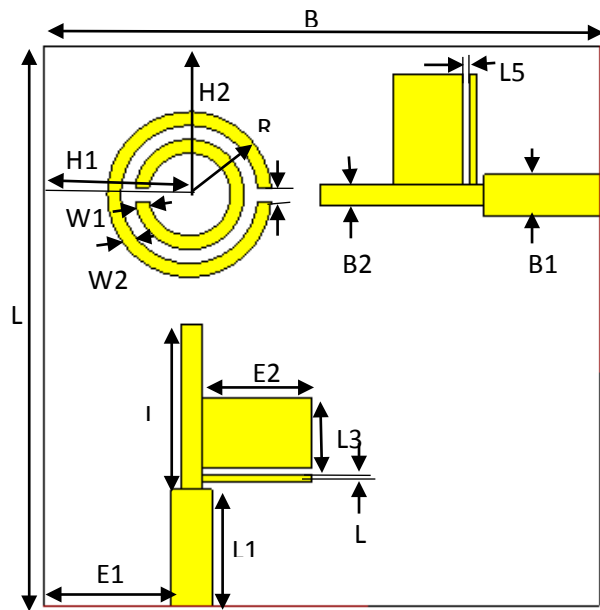
$$\theta_g = \arcsin \left(\frac{g}{2R} \right)$$

The total capacitance is calculated assuming that the gap and surface capacitances are placed in parallel.

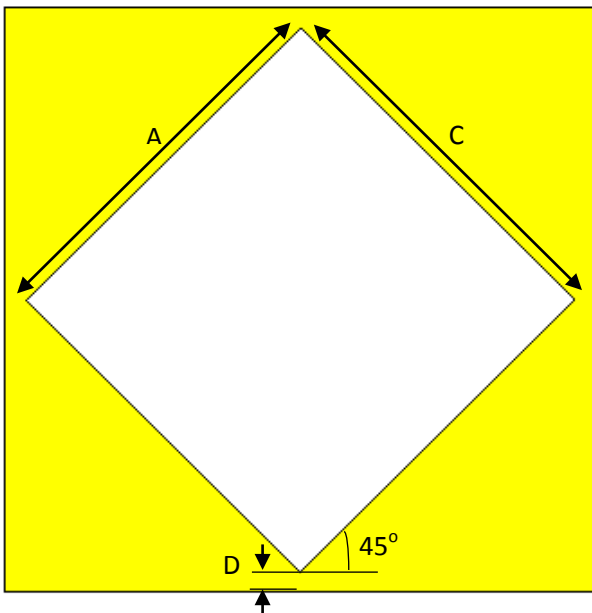
$$C = C_{gap} + C_{surf} \quad [21]$$

Once the frequency is calculated, the impedance bandwidth is widened to achieve the ultra-wideband frequency range. The disadvantages of using metamaterials are that it has limited bandwidth, complex antenna geometry, low efficiency, and it has no standard design procedure.

A planar inverted F UWB MIMO antenna is proposed in the 3.1 to 10.6 GHz frequency range with a split ring resonator which acts as a metamaterial. The top and bottom layer of the antenna is as shown in Fig. 39. The antenna is fabricated on an FR4 substrate with dielectric loss tangent 0.02, relative permittivity of 4.3 and with height 1.6 mm. The dimensions of the antenna are 38.5x38.5 mm. The antenna elements are placed perpendicular to each other and orthogonal polarization is exploited.



(a)



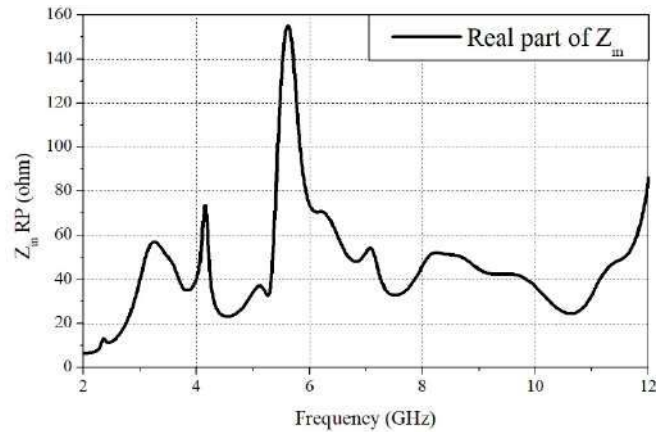
(b)

Fig.39 (a) Top and (b) Bottom of the antenna

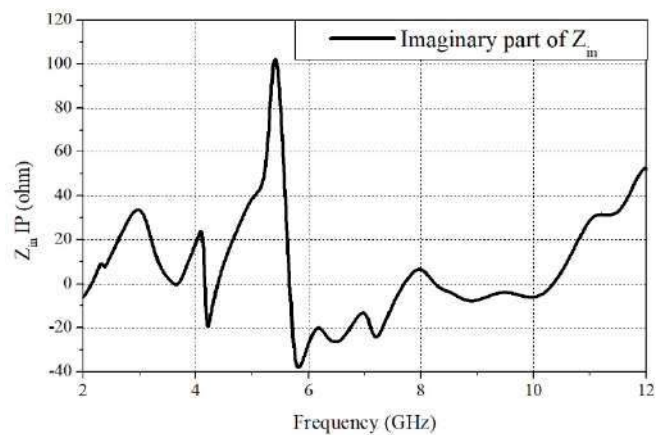
L	B	L1	L2	B1	B2	L3
38.5	38.5	8.4	12	3	1.5	5
A	C	W1	W2	R	G	D
18.8	18.8	1	1	6	1	1.45
E1	E2	H1	H2	L4	L5	
8.25	8	9.6	9.7	0.4	8	

a. Equivalent circuit

The real part of the input impedance of S_{11} of the UWB MIMO antenna is shown in Fig. 40(a). From the real part of input impedance of S_{11} from Fig. 40(a), it can be seen that the resonant peaks (parallel resonant modes) are at 3.26 GHz, 4.13 GHz, 5.26 GHz, 5.62 GHz, 7.09 GHz and at 8.29 GHz in the UWB and each frequency is represented as a parallel RLC circuit connected in series. From the imaginary part of the simulated impedance graph of Fig. 40(b), it can be seen that the band notch is at 5.42 GHz. At this frequency, the imaginary component is inductive with high resistance values, showing similar behavior of a parallel RLC circuit. Fig. 41 represents the equivalent circuit of the proposed UWB MIMO fractal antenna.



(a)



(b)

Fig. 40 (a) Real part and (b) Imaginary part of input impedance

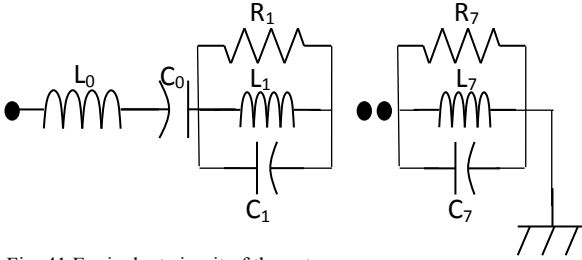


Fig. 41 Equivalent circuit of the antenna

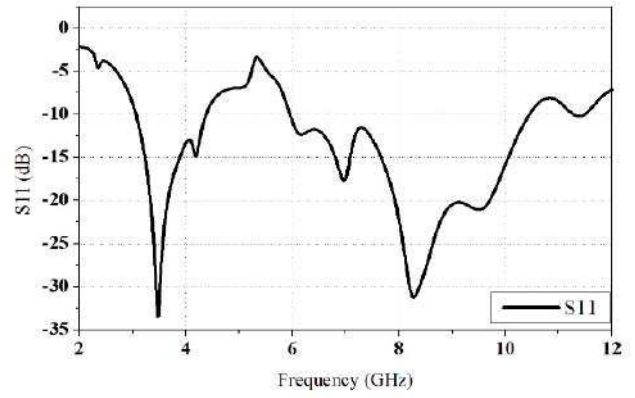
The parameters of the resistors, capacitors, and inductors in the equivalent circuit are as shown in Table. 7 and are obtained using foster canonical forms. The parallel RLC network acts as a bandpass filter, thus creating a resonance and the series RLC network acts as a band reject filter, thus rejecting the required frequency. A combination of the series RLC network and the parallel RLC network gives the desired UWB.

Frequency (GHz)		3.26	4.13	5.26
R_n (Ω)		56.75	70.76	63.16
L_n (nH)	0.38	6.03	6.34	1.96
C_n (pF)	1.45	3.95	2.34	46.70
Frequency (GHz)	5.42	5.62	7.09	8.29
R_n (Ω)	101.95	155.29	53.69	51.89
L_n (nH)	2.98	8.04	4.03	2.51
C_n (pF)	28.94	0.99	1.25	1.46

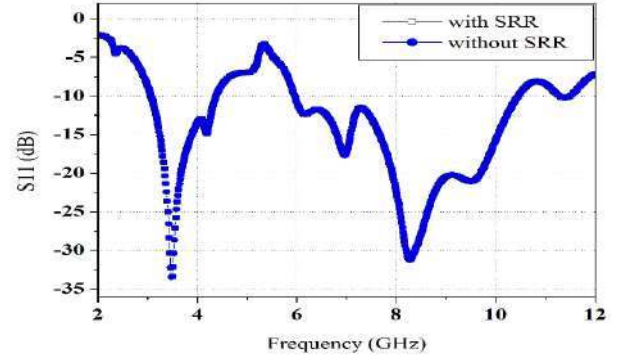
Table 7: Element values of the equivalent circuit

b. Simulated results

A rectangular slot defects in the ground plane and it behaves as a defected ground structure. The split ring resonator (SRR), which is introduced between the antenna elements improves the isolation in the lower band of the UWB frequency range. The antenna rejects the frequencies in the WLAN band. The antenna resonates as shown in Fig. 24 (a) in the 3.1 to 10.4 GHz UWB frequency range with $S_{11} < -10$ dB as shown in Fig. 42(a). A comparison of the graph obtained before and after the addition of the split ring resonator is as shown in Fig. 42(b). It can be observed that there is no change in the S_{11} obtained. The isolation obtained is greater than -20 dB in the desired band of interest as shown in Fig. 43(a) but there is an improvement in isolation with the introduction of split ring resonator as shown in Fig. 43(b). There is an isolation enhancement of 5 dB. The isolation of the antenna can be analyzed as follows: The split ring resonator induces a capacitance due to the gap in the rings and an inductance due to the ring structure. The combination of the capacitance and inductance creates a band stop filter and reduces the coupling between the antenna elements.

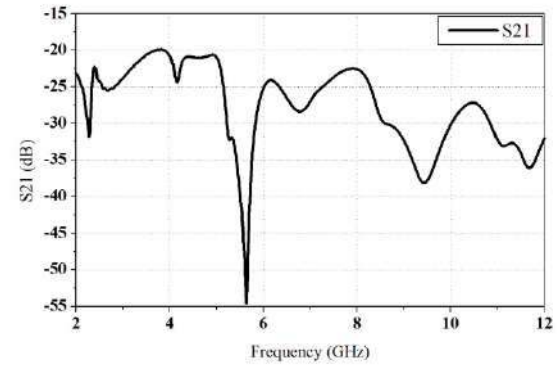


(a)

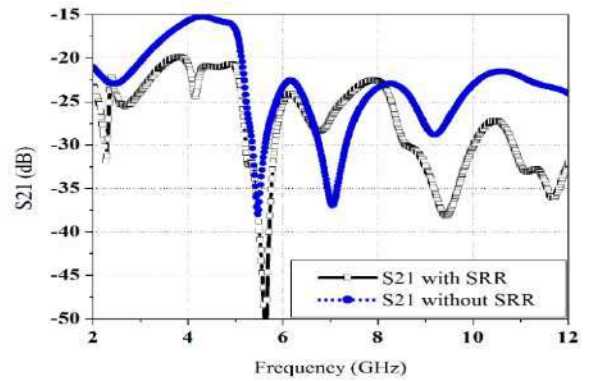


(b)

Fig.42 (a) S_{11} of the antenna and (b) Comparison of S_{11} with and without SRR



(a)



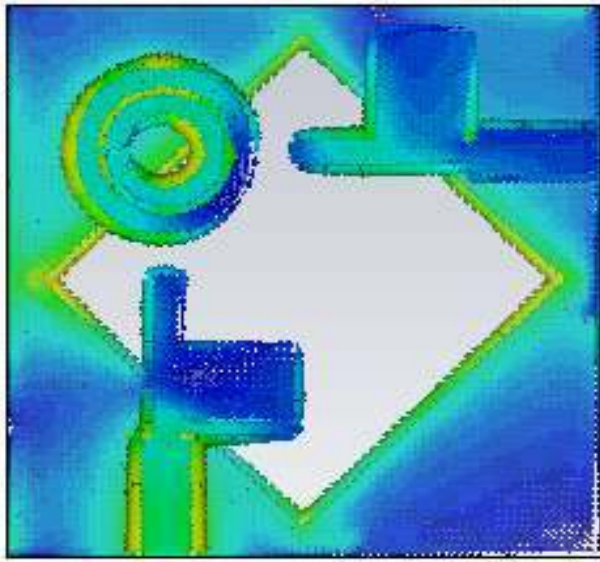
(b)

Fig. 43 (a) S_{21} of the antenna and (b) comparison of the mutual coupling with and without SRR

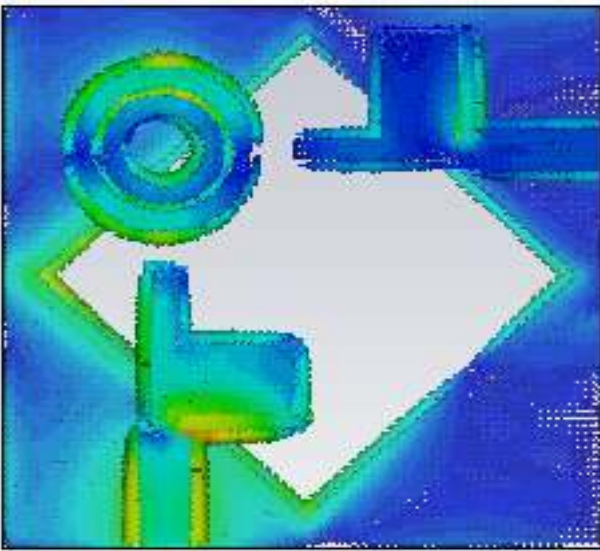
At 4 GHz, the split ring resonator behaves as a band reject filter and suppresses the current and improves the isolation. The defected ground structure also acts as a

band reject filter and further improves the isolation. The surface currents are mainly concentrated along the lower slit of the inverted-F antenna at 7.5 GHz as shown in Fig. 44. There is current flow along the split ring resonator in the +ve x-direction.

The ECC obtained is nearly equal to zero as shown in Fig. 45(a) in the ultra-wideband frequency range and the diversity gain obtained varies from 9.9-10 in the 3.1 to 6.5 GHz frequency range as shown in Fig. 45(b) and nearly 10 dB in the other higher frequency range. it shows good diversity performance. Although there is an increase in ECC in the lower band, the ECC is nearly equal to zero in the upper band from 6.5 GHz to 10.6 GHz. The Maximum gain obtained is greater than 5 dBi as shown in Fig. 45(c).

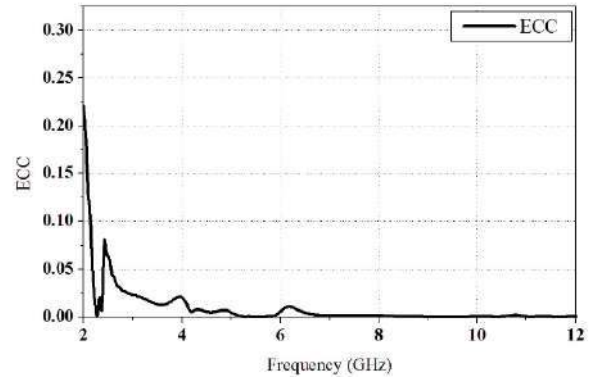


(a)

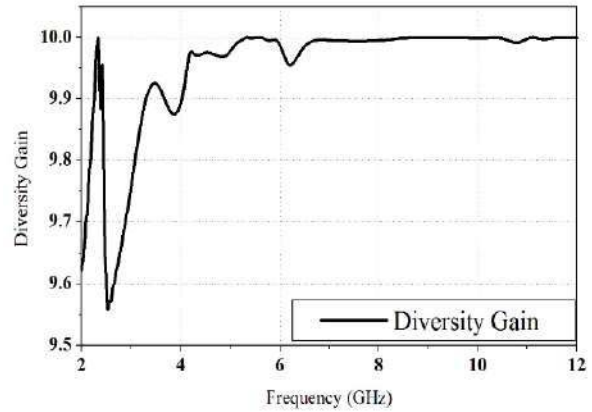


(b)

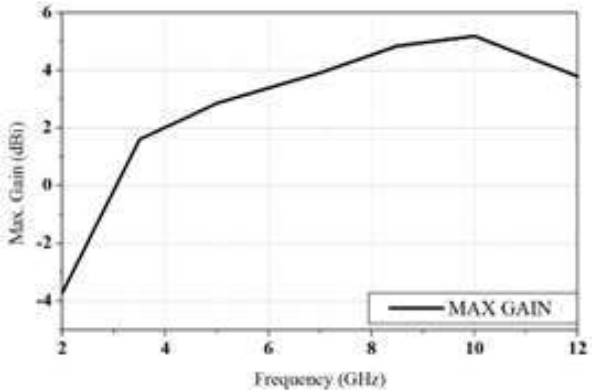
Fig. 44 The surface current distribution at port_1 at (a) 4 GHz and at (b) 7.5 GHz of the antenna



(a)



(b)



(c)

Fig. 45 (a) the ECC of the metamaterial based antenna (b) the Diversity gain and (c) the Maximum gain of the antenna

There are UWB-MIMO antennas that use metamaterials to enhance the isolation between the antenna elements. In [31], the antenna achieves high isolation and it also achieves band notching using metamaterials. The split ring resonator acts as an isolator and this SRR effectively restrains the radiation as it is loaded on the major radiation area than being etched around the feed point. The isolation obtained is higher than 17 dB in the ultra-wideband operation.

Antennas having a band gap structure are also classified as metamaterials-based antennas. EBG materials suppress the surface wave and it has the ability to permit electromagnetic wave propagation in certain bands which are also called as bandgaps. They have very good isolation properties but not in terms of radiated power as some energy is trapped in the bandgaps. EBGs structures are both metallic and dielectric elements. They are mainly used in

printed circuit boards to suppress surface waves and the metallo dielectric structures that are widely used are made of up periodic array of patches which are connected or are separated from each other.

Some of the bandgap structures in the literature for the UWB – MIMO antennas are, in [32], a planar monopole MIMO antenna is proposed which consists of a three slit-patch structure in the ground plane. The EBG structure uses two closely coupled arrays, in which one array consists of linearly conducting patches and the second array consists of slits in the ground plane. But the mechanism of the EBG structure is not explained. The isolation obtained is greater than 20 dB.

In [33], the antenna elements are having the dimensions of a staircase structure with a comb-like structure in the ground plane, to enhance the isolation. The coupling is suppressed between the antenna elements due to the presence of the comb-like structure which acts as an electromagnetic bandgap structure. The comb-like structure increases the isolation because of two different mechanisms. Firstly, the stubs on the ground plane suppress the ground current and secondly, the stubs are linked by a small metal strip which behaves as an EBG structure and forms a comb-like structure on the ground plane of the antenna and further reduces the isolation. The isolation obtained is greater than 25 dB and the ECC obtained is less than 0.001.

X. RECONFIGURABLE ANTENNAS

A study on UWB MIMO antennas will not be complete without a brief review on reconfigurable antennas. MIMO antennas having frequency reconfigurable properties are an important area of research. And it has been extended to the ultra-wideband range. The required frequency in the ultra-wide frequency range from 3.1 to 10.6 GHz is obtained using frequency reconfigurable antennas and switching between the various band reject bands also takes place using reconfiguration.

In [34], a two-element MIMO reconfigurable antenna is proposed for ultra-wideband applications. The antenna elements have a modified square structure. Each radiating patch is chamfered at the edges to improve the impedance bandwidth. An efficient decoupling structure which consists of 4 C-shaped strips which are layered between 3 vertical stubs in the ground plane is used to improve the isolation between the antenna elements. The C-shaped strips act as half-wavelength resonators. The isolation obtained is greater than 20 dB due to the presence of the defected ground structure in the ground plane. By orthogonally placing the antenna elements which leads to corner installation or by placing the antenna elements back-to-back to introduce three-dimensional modules which are compact in size, reconfiguration can be obtained. But reconfiguration does not take place due to switches. The proposed MIMO antenna achieves high isolation of 20 dB and the ECC obtained is less than 0.025.

In [35], a frequency reconfigurable UWB MIMO antenna, which rejects all WLAN in the frequency range 4.8 to 6.2 GHz is proposed where the antenna elements consist of two monopole elements, with a U-shaped slot introduced to improve the isolation. A $\lambda/4$ wave stub is introduced in the ground plane and a p-i-n diode is used for reconfiguration and it rejects the band gap. The shorting strip can be placed between the various ground plane and this gives another structure of the antenna. The elements are

placed orthogonal to each other to exploit polarization diversity. This mechanism improves the isolation. The length of the stubs is calculated as $L_{b1} = L_{b2} = \lambda/4 = c/(4f_0\sqrt{\epsilon_r})$ where $f_0 = 5.5$ GHz is the resonant frequency of the band that was rejected and the substrate has a relative permittivity of ϵ_r . When the diodes are in the ON state, a capacitance effect is obtained due to the gap between the stubs and the ground plane and a band stop resonator is obtained due to the stubs which results in a band- stop filter. The isolation obtained is greater than 20 dB.

XI. COMPARISON OF THE DIFFERENT ANTENNA STRUCTURES

From the review of isolation methods of UWB – MIMO antenna, it can be seen that using parasitic elements in a MIMO antenna gives maximum isolation. The isolation obtained using parasitic elements is 35 dB. This can be considered as the best technique for isolation enhancement between the antenna elements. The ECC of the elements is also nearly equal to zero. The capacity loss of the parasitic element technique is also very less with a value equal to 0.066 as shown in Table. 8. The capacity of the channel should be maximum but there is a loss in capacity due to correlation and coupling between the antenna elements. As the coupling between the elements is very less or the isolation is high and the capacity loss is also very low, we can conclude that the capacity of the channel is high.

Introducing orthogonal polarization also reduces the isolation between the antenna elements. The isolation obtained using parasitic elements is 35 dB and it better than the orthogonal polarization by 10 dB. Introducing split ring resonator and neutralization line between the antenna elements are also good techniques for the improvement of isolation between the antenna elements. Using split ring resonator and neutralization line also gives an isolation which is 5 dB better than the minimum value (i.e. 15 dB) required for coupling in a MIMO antenna.

The envelope correlation coefficient obtained for all the above-mentioned antennas are excellent and is nearly close to zero in the required UWB frequency range. This indicates that the UWB MIMO antennas are suitable for practical applications with good diversity performance. The diversity gain is another technique to characterize the antenna performance. The diversity gain of the antenna is nearly equal to 10 dB in all the antennas.

The capacity loss gives the amount of loss in the capacity when the antenna elements are correlated. All antennas are correlated to some extent as there is a correlation in the radiation patterns of the antenna elements. The amount of capacity loss should be very low. The capacity loss of the antenna for various antennas is as given in Table. 8. The method using parasitic elements gives very low capacity loss of 0.0229. The antennas with the decoupling structure and the defected ground structure give a minimum capacity loss giving a value of 0.043. All the other antennas also give low capacity loss as the loss is less than 0.5. This shows that the capacity loss is below the reference value of 0.5. The maximum value of gain for the UWB MIMO antennas is in the range of 4 – 5 dBi and the technique using orthogonal polarization gives the highest value of 6 dBi.

Types of antenna	Dimensions (mm ²)	S11 (dB)	Bandwidth (dB)	Fractional Bandwidth	S21 (dB)	ECC	Capacity loss (bits/s/Hz)	Maximum Gain (dBi)
Orthogonal polarization	39.8x23	2.2 - 12	9.8	1.38	-25	0	0.39	6
Parasitic element	38.5x38.5	2.8 - 10.6	7.8	1.16	-35	0	0.066	4
Decoupling structure	33x45.5	3.1 - 10.6	7.5	1.09	-15	0	0.043	4
Defected ground structure_1	24x18	2 - 12	10	1.43	-15	0.025	0.043	4
Defected Ground Structure_2	22x32	3.1 - 12	8.9	1.17	-22	0.3	0.243	5
Neutralization line	40x80	2.8 - 12	9.2	2	-20	0	0.029	5
Metamaterial	38.5x38.5	2 - 10.6	8.6	1.36	-20	0	0.358	5

Table 8. Comparison of the different isolation techniques

XII. CONCLUSION

There is a lot of research work going on around the globe on UWB – MIMO antenna. But research has to be done in further improving the isolation between the antenna elements. A study of the various isolation enhancement techniques has been made in this review. It analyses the various isolation enhancement methods such as using orthogonal polarization, parasitic elements, varied decoupling structures, defected ground structures, neutralization line and finally by using metamaterials. Metamaterials is a technology to improve the isolation between the antenna elements. Split ring resonator behaves as a metamaterial and it used as an isolation mechanism in this study. The antennas are simulated and the results are compared. The method using parasitic elements gives the higher isolation of 35 dB and it is 5 dB better than the methods using orthogonal polarization and using the decoupling structure. The performance of all the antennas satisfies the conditions for minimum isolation. The envelope correlation coefficient is nearly zero in all the antennas and it implies good diversity performance. The bandwidth of the antennas is in the UWB frequency range and they have a fractional bandwidth above the required value of 1.09. The capacity loss for all the antennas is very low and the antennas using defected ground structure and the decoupling structure gives a very low capacity loss. The maximum gain for the UWB MIMO antennas is in the range 4 – 5 dBi. The technique using orthogonal polarization gives the maximum value of 6 dBi.

REFERENCES

- [1] M.S Sharawi, Printed MIMO Antenna Engineering, Artech House, 2012.
- [2] Lee, W.-S., D.-Z. Kim, K.-J. Kim, and J.-W. Yu, "Wideband planar monopole antennas with dual band-notched characteristics," *IEEE Trans. Microwave Theory Tech.*, Vol. 56, No. 12, 3637-3644, Dec. 2008.
- [3] Jianfeng Zhu, Shufang Li, Botao Feng, Li Deng, and Sixing Yin. "Compact dual-polarized UWB quasi-self-complementary MIMO/diversity antenna with band-rejection capability," *IEEE Antennas and Wireless Propagation Letters*, Vol. 15, pp. 905-908, 2016.
- [4] Muhammad Saeed Khan, Antonio-Daniele Capobianco, Adnan Iftikhar, Raed M. Shubair, Dimitris E. Anagnostou, and Benjamin D. Braaten. "Ultra-compact dual-polarised UWB MIMO antenna with meandered feeding lines." *IET Microwaves, Antennas & Propagation*, Vol. 11, no. 7, pp. 997-1002, 2017.
- [5] Gunjan Srivastava, and Akhilesh Mohan. "Compact MIMO slot antenna for UWB applications." *IEEE Antennas and Wireless Propagation Letters* Vol. 15, pp.1057-1060, 2016.
- [6] M. S.Khan, A. D. Capobianco, S. Asif, A. Iftikhar, B. Ijaz, and B. D. Braaten. "Compact 4× 4 UWB-MIMO antenna with WLAN band rejected operation." *Electronics Letters*, vol. 51, no. 14, pp.1048-1050, 2015.
- [7] Muhammad Saeed Khan, Antonio-Daniele Capobianco, Aftab Naqvi, Bilal Ijaz, Sajid Asif, and Benjamin D. Braaten. "Planar, compact ultra-wideband polarization diversity antenna array." *IET Microwaves, Antennas & Propagation*, Vol. 9, no. 15 pp. 1761-1768, 2015.
- [8] Jae-Min Lee, Ki-Baek Kim, Hong-Kyun Ryu, and Jong-Myung Woo. "A compact ultrawideband MIMO antenna with WLAN band-rejected operation for mobile devices." *IEEE Antennas and Wireless Propagation Letters*, Vol.11, pp.990-993, 2012.
- [9] Le Kang, Hui Li, Xinhui Wang, and Xiaowei Shi. "Compact offset microstrip-fed MIMO antenna for band-notched UWB applications." *IEEE Antennas and Wireless Propagation Letters*, Vol.14, pp.1754-1757, 2015.
- [10] Cheng-Hsun Wu, Chia-Lin Chiu, and Tzyh-Ghuang Ma. "Very compact fully lumped decoupling network for a coupled two-element array." *IEEE Antennas and Wireless Propagation Letters*, Vol.15, pp. 158-161, 2016.
- [11] Muhammad Saeed Khan, Antonio-Daniele Capobianco, Ali Imran Najam, Imran Shoaib, Elena Autizi, and Muhammad Farhan Shafique. "Compact ultra-wideband diversity antenna with a floating parasitic digitated decoupling structure." *IET Microwaves, Antennas & Propagation*, Vol.8, no. 10, pp.747-753, 2014.
- [12] Shuai Zhang, Zhinong Ying, Jiang Xiong, and Sailing He. "Ultrawideband MIMO/diversity antennas with a tree-like structure to enhance wideband isolation." *IEEE Antennas and Wireless Propagation Letters*, Vol.8, pp. 1279-1282, 2009.
- [13] R. Saleem, M. Bilal, K. B. Bajwa, and M. F. Shafique. "Eight-element UWB-MIMO array with three distinct isolation mechanisms." *Electronics Letters*, Vol.51, no. 4, pp. 311-313, 2015.
- [14] Li Liu, S. W. Cheung, and T. I. Yuk. "Compact MIMO antenna for portable UWB applications with band-notched

- characteristic." *IEEE Transactions on Antennas and Propagation* Vol.63, no. 5, pp.1917-1924, 2015.
- [15] Li Liu, Sing, Wai Cheung, and Tung Ip Yuk. "Compact multiple-input–multiple-output antenna using quasi-self-complementary antenna structures for ultrawideband applications." *IET Microwaves, Antennas & Propagation* Vol.8, no. 13, pp. 1021-1029, 2014.
- [16] Shuai Zhang, Buon Kiong Lau, Anders Sunesson, and Sailing He. "Closely-packed UWB MIMO/diversity antenna with different patterns and polarizations for USB dongle applications." *IEEE Transactions on Antennas and Propagation*, Vol.60, no. 9, pp. 4372-4380, 2012.
- [17] Jian Ren, Wei Hu, Yingzeng Yin, and Rong Fan. "Compact printed MIMO antenna for UWB applications." *IEEE antennas and wireless propagation letters*, Vol. 13, pp. 1517-1520, 2015.
- [18] Jian Ren, Dawei Mi, and Ying-Zeng Yin. "Compact ultrawideband MIMO antenna with WLAN/UWB bands coverage." *Progress In Electromagnetics Research C*, Vol.50,pp.121-129, 2014.
- [19] R.V.S.Ram Krishna, and Raj Kumar. "A dual-polarized square-ring slot antenna for UWB, imaging, and radar applications." *IEEE Antennas and Wireless Propagation Letters*, Vol.15, pp. 195-198, 2016.
- [20] R.Chandel, and A. K. Gautam. "Compact MIMO/diversity slot antenna for UWB applications with band-notched characteristic." *Electronics Letters* Vol.52, no. 5, pp.336-338, 2015.
- [21] H.F.Huang, and Shu-Guang Xiao. "Compact triple band-notched UWB MIMO antenna with simple stepped stub to enhance wideband isolation." *Progress In Electromagnetics Research Letters*, Vol.56, pp. 59-65, 2015.
- [22] Jing-Yi Zhang, Fan Zhang, Wen-Peng Tian, and Yong-Lun Luo. "ACS-fed UWB-MIMO antenna with shared radiator." *Electronics Letters*, Vol.51, no. 17, pp. 1301-1302, 2015.
- [23] Li Liu, Li, S. W. Cheung, and T. I. Yuk. "Compact MIMO antenna for portable devices in UWB applications." *IEEE Transactions on Antennas and Propagation*, Vol.61, no. 8, pp. 4257-4264, 2013.
- [24] Shrivishal Tripathi, Akhilesh Mohan, and Sandeep Yadav. "A compact Koch fractal UWB MIMO antenna with WLAN band-rejection." *IEEE Antennas and wireless propagation letters*, Vol.14, pp. 1565-1568, 2015.
- [25] Peng Gao, Shuang He, Xubo Wei, Ziqiang Xu, Ning Wang, and Yi Zheng. "Compact printed UWB diversity slot antenna with 5.5-GHz band-notched characteristics." *IEEE Antennas and Wireless Propagation Letters*, Vol.13, pp. 376-379, 2013.
- [26] Bybi P Chacko, Gijo Augustin, and Tayeb A. Denidni. "Uniplanar polarisation diversity antenna for ultra-wideband systems." *IET Microwaves, Antennas & Propagation*, Vol.7, no. 10, pp. 851-857, 2015.
- [27] Jian-Feng Li, Qing-Xin Chu, Zhi-Hui Li, and Xing-Xing Xia. "Compact dual band-notched UWB MIMO antenna with high isolation." *IEEE transactions on antennas and propagation*, Vol.61, no. 9, pp. 4759-4766, 2013.
- [28] T. K. Roshna, U. Deepak, V. R. Sajitha, K. Vasudevan, and P. Mohanan. "A compact UWB MIMO antenna with reflector to enhance isolation." *IEEE Transactions on Antennas and Propagation* Vol. 63, no. 4, pp. 1873-1877, 2015.
- [29] M. Gulam Nabi Alsath, and Malathi Kanagasabai. "Compact UWB monopole antenna for automotive communications." *IEEE Transactions on Antennas and Propagation* Vol. 63, no. 9, pp. 4204-4208, 2015.
- [30] Yantao Yu, Xiaoya Liu, Zhaokai Gu, and Lijun Yi. "A compact printed monopole array with neutralization line for UWB applications." In *IEEE International Symposium on Antennas and Propagation (APSURSI)*, 2016, pp. 1779-1780, 2016.
- [31] Fei Wang , Zhaoyun Duan, Tao Tang, Minzhi Huang, Zhanliang Wang, and Yubin Gong. "A new metamaterial-based UWB MIMO antenna." *IEEE International In Wireless Symposium (IWS)*, 2015, pp. 1-4, 2015.
- [32] Qian Li, Alexandros P. Feresidis, Marina Mavridou, and Peter S. Hall. "Miniaturized double-layer EBG structures for broadband mutual coupling reduction between UWB monopoles." *IEEE Transactions on Antennas and Propagation*, Vol.63, no. 3, pp. 1168-1171, 2015.
- [33] Narges Malekpour, and Mohammad Amin Honarvar. "Design of high-isolation compact MIMO antenna for UWB application." *Progress In Electromagnetics Research C*, Vol.62, pp. 119-129, 2016.
- [34] Irum Jafri, Syeda Rashid Saleem, Muhammad Farhan Shafique, and Anthony Keith Brown. "Compact reconfigurable multiple-input-multiple-output antenna for ultra wideband applications." *IET Microwaves, Antennas & Propagation*, Vol.10, no. 4, pp. 413-419, 2016.
- [35] Khan, M. S., A. D. Capobianco, A. Naqvi, M. F. Shafique, B. Ijaz, and B. D. Braaten. "Compact planar UWB MIMO antenna with on-demand WLAN rejection." *Electronics Letters*, Vol.51, no. 13, pp. 963-964, 2015. Khan, M. S., A. D. Capobianco, A. Naqvi, M. F. Shafique, B. Ijaz, and B. D. Braaten. "Compact planar UWB MIMO antenna with on-demand WLAN rejection." *Electronics Letters*, Vol.51, no. 13, pp. 963-964, 2015.
- [36] I. Pele, A. Chousseaud, and S. Toutain. "Simultaneous modeling of impedance and radiation pattern antenna for UWB pulse modulation." In *Antennas and Propagation Society International Symposium*, 2004. IEEE, vol. 2, pp. 1871-1874. IEEE, 2004. DOI: 10.1109/APS.2004.1330566
- [37] H-J Zhou, B-H. Sun, Q-Zh Liu, and J-Y. Deng. "Implementation and investigation of U-shaped aperture UWB antenna with dual band-notched characteristics." *Electronics letters* vol. 44, no. 24, pp. 1387-1388, 2008. DOI: 10.1049/el:20082661
- [38] Gnanaharan Irene, and Anbazhagan Rajesh. "A Penta-Band Reject Inside Cut Koch Fractal Hexagonal Monopole UWB MIMO Antenna for Portable Devices." *Progress In Electromagnetics Research* 82 (2018): 225-235. 2018 accepted, in press.
- [39] Constantinos Votis, George Tatsis, and Panos Kostarakis. "Envelope correlation parameter measurements in a MIMO antenna array configuration." *International Journal of Communications, Network and System Sciences* vol. 3, no. 04, pp. 350-354, 2010. DOI:10.4236/ijcns.2010.34044.